Online Research @ Cardiff

This is an Open Access document downloaded from ORCA, Cardiff University's institutional repository: https://orca.cardiff.ac.uk/id/eprint/122349/

This is the author's version of a work that was submitted to / accepted for publication.

Citation for final published version:

Van Tuyl, James, Alves, Tiago ORCID: https://orcid.org/0000-0002-2765-3760, Cherns, Lesley ORCID: https://orcid.org/0000-0002-9052-3213, Antonatos, Georgios, Burgess, Peter and Masiero, Isabella 2019. Geomorphological evidence of carbonate build-up demise on equatorial margins: A case study from offshore northwest Australia. Marine and Petroleum Geology 104 , pp. 125-149. 10.1016/j.marpetgeo.2019.03.006 file

Publishers page: http://dx.doi.org/10.1016/j.marpetgeo.2019.03.006 <http://dx.doi.org/10.1016/j.marpetgeo.2019.03.006>

Please note:
Changes made as a result of publishing processes such as copy-editing, formatting and page numbers may not be reflected in this version. For the definitive version of this publication, please refer to the published source. You are advised to consult the publisher's version if you wish to cite this paper.

This version is being made available in accordance with publisher policies. See http://orca.cf.ac.uk/policies.html for usage policies. Copyright and moral rights for publications made available in ORCA are retained by the copyright holders.

information services
gwasanaethau gwybodaeth

Marine and Petroleum Geology 104 (2019) 125–149

Contents lists available at ScienceDirect

Marine and Petroleum Geology

journal homepage: www.elsevier.com/locate/marpetgeo

Research paper

Geomorphological evidence of carbonate build-up demise on equatorial margins: A case study from offshore northwest Australia

James Van Tuyl[a,*], Tiago Alves[a], Lesley Cherns[a], Georgios Antonatos[b], Peter Burgess[c], Isabella Masiero[c]

[a] 3D Seismic Lab, School of Earth and Ocean Sciences, Cardiff University, Main Building, Park Place, CF10 3AT, Cardiff, United Kingdom
[b] School of Earth Sciences, Royal Holloway, University of London, Egham, Surrey, TW20 0EX, United Kingdom
[c] Department of Earth, Ocean and Ecological Sciences, University of Liverpool, Jane Herdman Building, 4 Brownlow Street, Liverpool, L69 3GP, United Kingdom

ARTICLE INFO

Keywords:
Equatorial margins
Northwest Australia
Miocene
Carbonate shelf
Build-up
Demise

ABSTRACT

The demise of Miocene carbonate build-ups in the Browse Basin, Northwest Australia, has been explained as relating to geological and oceanographic processes. These include accelerated tectonic subsidence driven by subduction, ocean cooling following the mid-Miocene climate optimum, nutrient excess, poisoning by sediment drifts and local erosion driven by current winnowing, occurring discretely or simultaneously. Here, we critically assess the evidence for these different mechanisms using a combination of high-resolution 3-D seismic data, regional 2-D seismic profiles, and numerical stratigraphic forward modelling. Seismic interpretation and numerical modelling found that the proposed uniform subsidence rate of 125 m/Ma between 16.5 Ma and 5.33 Ma for the northern Browse Basin (Belde et al., 2017), when combined with the published estimate of eustatic sea level in Miller et al. (2005), was insufficient to drown the Miocene carbonate sequence and generate the geomorphological changes (barrier reef to isolated carbonate build-ups) observed on seismic data. Instead, a subsidence profile comprising pulses of rapid and slow subsidence is required. Significantly, our results suggest that subsidence rates exceeded 400 m/Ma in the northern Browse Basin, and that parts of the basin record the accumulation of sediment drifts. These sediment drifts are interpreted to have buried some carbonate build-ups, while suspended sediment reduced light transmissivity, inhibiting carbonate production. Thus, we postulate that current activity and excess nutrient supply are key, but often overlooked, oceanographic processes that lead to the demise of carbonate build-ups.

1. Introduction

Drowned carbonate build-ups are common throughout the Phanerozoic geological record (Schlager, 1981; Hallock and Schlager, 1986). The drowning of carbonate build-ups is defined as an event in which relative sea-level rise - the sum of tectonic and eustatic movements - outpaces sediment accumulation to submerge the carbonate factory below the euphotic zone. However, Schlager (1981) found healthy carbonate production to be some orders of magnitude greater than long-term rises in sea level, introducing an important scientific 'paradox' regarding the drowning of carbonate reefs and platforms. According to Schlager (1981), long-term rises in sea level are unlikely to drown carbonate platforms unless changes in relative sea level occur as rapid pulses on 100,000 years to 1 Ma timescales. Such timescales can be the result of regional faulting or inter-glacial periods, but they are seldom recorded on carbonate platforms across the world.

Recent data have shown that environmental decline suppresses carbonate production at the scale of a continental margin, making carbonate build-ups more susceptible to small-scale relative sea-level rises (Hallock, 2006; Kim et al., 2012; Woodroffe and Webster, 2014). The suppression of carbonate production can occur through a number of processes. First, siliciclastic input can rapidly bury carbonate build-ups in some areas, while suspended sediment decreases the light transmissivity of the water column below the values required by carbonate-producing organisms. Second, carbonate production declines in ocean temperatures below certain optimum values, e.g. below 24 °C for modern tropical carbonates. This reduces carbonate production rates, or favours carbonate organisms that do not build structures capable of matching relative sea-level rises (Isern et al., 1996; Brachert et al., 2006). Third, changes in ocean composition (e.g. salinity) can stress carbonate-producing organisms (Schlager, 1981). Finally, excess nutrients (nitrates and phosphates) decrease water transparency and

* Corresponding author.
E-mail address: vantuylj@cardiff.ac.uk (J. Van Tuyl).

https://doi.org/10.1016/j.marpetgeo.2019.03.006
Received 2 January 2019; Received in revised form 1 March 2019; Accepted 6 March 2019
Available online 15 March 2019
0264-8172/ © 2019 The Authors. Published by Elsevier Ltd. This is an open access article under the CC BY license (http://creativecommons.org/licenses/BY/4.0/).

inhibit photosynthetic production, while also promoting the growth of fleshy algae and suspension-feeding animals. These suspension feeders are known to compete and displace hermatypic algae and corals (Hallock and Schlager, 1986).

In the Browse Basin, the demise of carbonate production is dated between ~10 Ma (Tortonian) and the Miocene-Pliocene boundary (~5.33 Ma) (Rosleff-Soerensen et al., 2016; Belde et al., 2017; Van Tuyl et al., 2018). This demise has been attributed to accelerated tectonic subsidence driven by subduction in the Timor Trough (Rosleff-Soerensen et al., 2012, 2016; Belde et al., 2017). Authors have also postulated that environmental decline in the form of ocean cooling following the mid-Miocene climate optimum (Isern et al., 1996), nutrient excess (Howarth and Alves, 2016), as well as sediment drifts and erosion driven by current winnowing (Belde et al., 2017), suppressed carbonate production to the point where it was unable to keep-up with relative sea-level rise. All these conceptual models are still subject to debate.

In this work, we use seismic interpretation, in conjunction with stratigraphic forward modelling (CarboCAT; Burgess, 2013), to test the current conceptual models for the growth and demise of a Miocene carbonate sequence in the northern Browse Basin, offshore Northwest Australia (Fig. 1). We test time-dependent processes (eustatic sea level, tectonics, and environmental decline) to investigate their significance in generating the growth patterns displayed by the carbonate build-ups of the northern Browse Basin on 3-D seismic data. This work furthers our understanding of the Miocene carbonate platforms offshore Northwest Australia, and its results can be applied globally to carbonate build-ups on Equatorial Margins. In summary, the main research questions addressed in this work include:

1) What was the relative significance of subsidence vs. eustatic sea-level change on Miocene carbonate evolution offshore Northwest Australia?
2) What was the primary control on the demise of carbonate build-ups offshore Northwest Australia?
3) What is the validity of CarboCAT numerical models in assisting the interpretation of carbonate sequences on 3-D seismic data?

2. Geological background

2.1. Meso-Cenozoic evolution of the Browse Basin

Lying at the southern end of the Timor Sea, the Browse Basin is an offshore sedimentary basin that covers an area of approximately 140,000 km^2 on Australia's North West Shelf, itself a northeast-striking rifted continental margin (Struckmeyer et al., 1998; Rosleff-Soerensen et al., 2012, 2016; Stephenson and Cadman, 1994) (Fig. 1). The Browse Basin underwent multi-stage deformation during Mesozoic rifting, followed by several episodes of thermal subsidence and tectonic inversion (Willis, 1988; Haston and Farrelly, 1993; Struckmeyer et al., 1998). This generated a series of margin parallel half-grabens that dip landwards (Struckmeyer et al., 1998; Rosleff-Soerensen et al., 2012). These

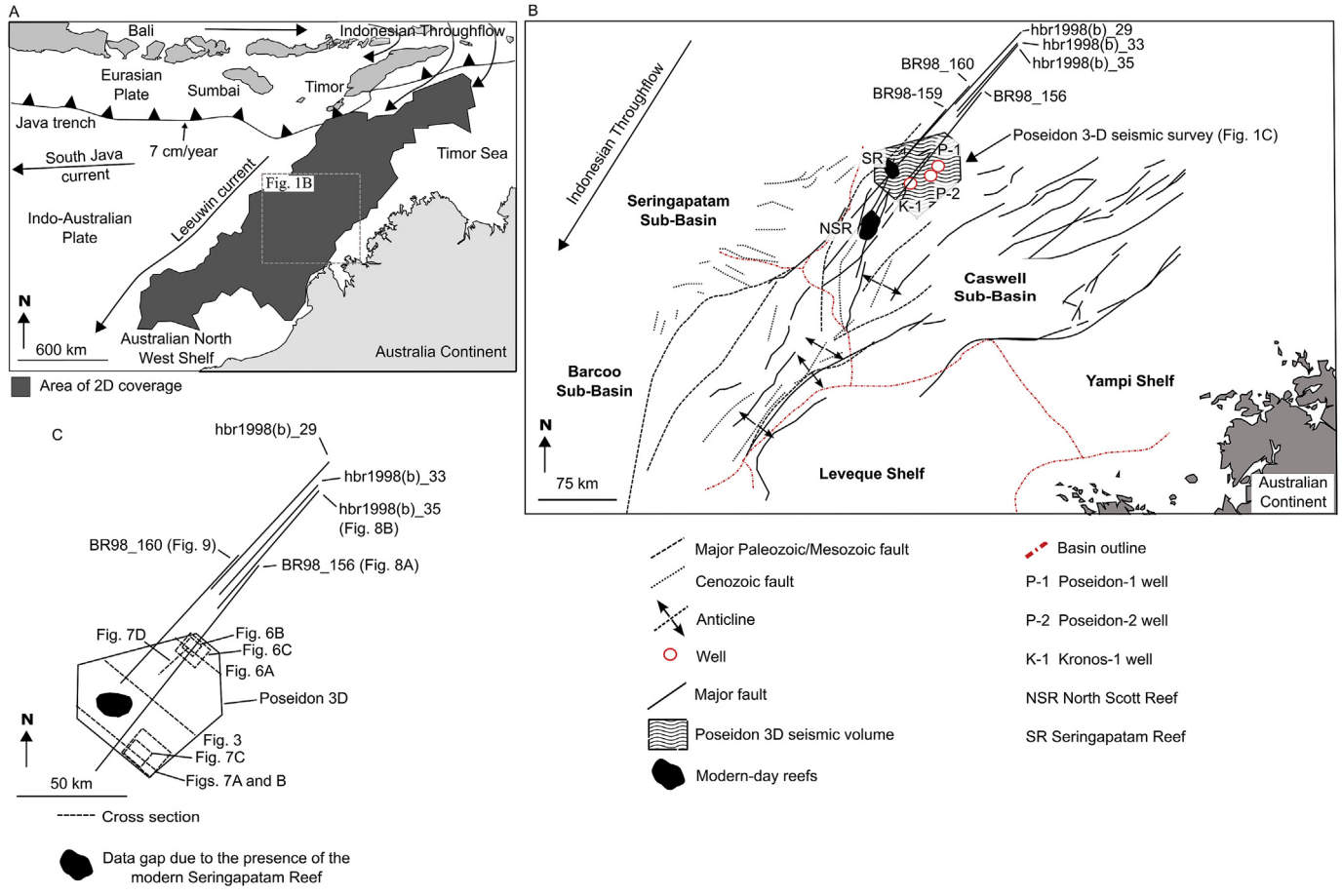

Fig. 1. (A) Regional map showing the location of the study area and the coverage of the 2-D seismic dataset on the Northwest Shelf relative to the orientation of major ocean currents. (B) Map of the Browse Basin showing the location of the Caswell and Barcoo sub-basins together with the main northeast-striking structural trends in the region. The location of the Poseidon 3-D seismic survey and regional 2-D seismic profiles interpreted in this work are also shown, as well as key exploration wells. (C) Regional extent of the 3-D Poseidon seismic survey showing the location of key seismic profiles and time-slices presented in this paper. The position of the modern day Seringapatam Reef is highlighted in the figure. Figure A is adapted from Blevin et al. (1998), Struckmeyer et al. (1998) and Rosleff-Soerensen et al. (2016). Figure B is adapted from Van Tuyl et al. (2018).

half-grabens were buried by a Lower Cretaceous sequence (Stephenson and Cadman, 1994; Struckmeyer et al., 1998; Langhi and Borel, 2007; Rosleff-Soerensen et al., 2012).

Seafloor spreading in the Indian and Southern Oceans drove the northward migration of the Australia continent from ~40°S in the Oligocene/Eocene to ~20°S at present (Apthorpe, 1988; Hull and Griffiths, 2002). Simultaneous anti-clockwise rotation of the Australian continent in the Late Oligocene-Early Miocene, due to oblique collision between the Pacific and Australasian plates (Veevers and Powell, 1984), promoted subsidence and shallow extensional faulting on the outer North West Shelf (Stephenson and Cadman, 1994; Howarth and Alves, 2016). At this same time, the synchronous reactivation of Jurassic (and older) faults was capable of amplifying Jurassic structures (Harrowfield and Keep, 2005; Rosleff-Soerensen et al., 2012) to generate moderate tectonic inversion in the Browse Basin (Keep et al., 2000).

2.2. Cenozoic evolution, stratigraphy and conceptual models of Miocene carbonate build-up demise

Cenozoic strata in the Browse Basin predominantly comprise temperate and tropical carbonates (Rosleff-Soerensen et al., 2012, 2016) (Figs. 2 and 3). A transition from ramp to rimmed-platform geometries is recorded at the end of the Paleogene (Apthorpe, 1988; Rosleff-Soerensen et al., 2012, 2016 Tesch et al., 2018). Hence, a regional unconformity marking the Oligocene-Miocene boundary documents a sharp change from a mid-ramp setting to a shallow-marine rimmed platform (Stephenson and Cadman, 1994; Saqab and Bourget, 2015). Overall, the Miocene carbonate sequence of the Browse Basin is regarded as aggradational (ConocoPhillips, 2012).

Van Tuyl et al. (2018) identified five sequence boundaries and four seismic stratigraphic units within the 1475 m-thick Miocene carbonate formation of the northern Browse Basin (Figs. 2 and 3). In the studied carbonate sequence, dated between ~16.5 ± 1 Ma and 4.8 Ma ± 1 Ma, Van Tuyl et al. (2018) documented tropical carbonate initiation above flat-topped bryozoan reefs (Fig. 3). Initial aggradation was followed by basinward migration of carbonate production from the latest Burdigalian-Langhian to the early Tortonian. The initial phase of progradation towards the northwest was restricted by the underlying topography of the Eocene carbonate ramp (Belde et al., 2017; Van Tuyl et al., 2018).

Progradation culminated in an extensive barrier-reef system along the basin margin, which first aggraded and subsequently drowned during the Late Tortonian, agreeing with the regional trend presented by Rosleff-Soerensen et al. (2012, 2016) and Belde et al. (2017). The Messinian growth patterns documented in Van Tuyl et al. (2018), showing progradational geometries and karst horizons that persisted on the basin margin, contrast with the observed retreat of carbonate build-ups onto inversion anticlines in the southern Browse Basin (Rosleff-Soerensen et al., 2016; Belde et al., 2017). Van Tuyl et al. (2018) suggested that the contrasting growth patterns in the northern Browse basin were due to the concentration of strain associated with plate collision in the Barcoo Sub-basin to the south of the study area, in line with Keep et al. (1998). This led to the reactivation of faults that were preferentially oriented in relation to the regional stresses, and these faults were mostly located in the southern portion of the Browse Basin.

Most authors have attributed the demise of the Browse Basin carbonate system, between ~10 Ma and the Miocene-Pliocene boundary (~5.33 Ma), to an acceleration of tectonic subsidence at that time (Rosleff-Soerensen et al., 2012). However, Rosleff-Soerensen et al. (2012, 2016), Howarth and Alves (2016) and Belde et al. (2017) also suggest environmental decline as responsible for the drowning of the studied carbonate build-ups. Global cooling after the Mid-Miocene climate optimum is not favoured as a mechanism for drowning in the Browse Basin; Karas et al. (2011) suggested that the expansion of the tropical warm pool in the early Pliocene generated sea-surface temperatures between 23 °C and 27 °C slightly south of the Browse Basin. Howarth and Alves (2016) proposed nutrient excess, driven by the progressive intensification of nutrient-rich Indonesian Throughflow (ITF) waters onto the continental shelf, as the main cause of build-up drowning in the Browse Basin. The flow of ITF waters promoted competition between carbonate factories and a net decrease in carbonate production. Belde et al. (2017) proposed the ITF to have the opposite effect, citing Quaternary reefs of the North West Shelf (Gallagher et al., 2014) as evidence for reduced nutrient volumes. Belde et al. (2017) proposed drift sedimentation and current winnowing to have inhibited the ability of production to keep up with relative sea-level rise in a manner similar to that proposed by Betzler et al. (2015, 2016).

3. Data and methods

3.1. 3-D Seismic dataset

This study uses the 2828 km^3 Poseidon three-dimensional (3-D) seismic volume and a series of 2-D seismic profiles that form part of a larger regional grid (Fig. 1). The Poseidon 3-D survey was acquired along sail lines oriented 130°/310° in the area adjacent to the Seringapatam Reef (ConocoPhillips, 2012), and parallel to the northwest-striking continental shelf. The dataset follows the SEG European polarity convention, i.e. an increase in acoustic impedance is represented as a red reflection on the interpreted seismic profiles (Fig. 3).

The interpreted dataset includes exploration wells Poseidon-1, Poseidon-2, and Kronos-1. Well Poseidon-1 is a wildcat and found gas in the Lower-Mid Jurassic Plover Formation (Fig. 1). It provides gamma-ray curves and rates of penetration from 494 to 5058 m true vertical depth sub-sea (m TVDSS), resistivity data from 560 to 5058 m TVDSS, and velocity data from 2299 to 4975 m TVDSS (ConocoPhillips, 2010). The Poseidon-2 appraisal well was drilled after the Poseidon-1 discovery to assess the presence and quality of gas in the Plover Formation. It provides gamma-ray and resistivity data from 556.9 to 5334.4 m TVDSS, velocity data from 2407.2 to 4702.2 m and lithologies from 2010 to 4053 m TVDSS (ConocoPhillips, 2011a; Howarth and Alves, 2016). The Kronos-1 well was also drilled to test for hydrocarbons within the Plover Formation. It provides formation tops, gamma-ray and resistivity data from 594.6 m TVDSS, as well as sonic velocity from 594.6 to 2033 m TVDSS and 2663–4778 m TVDSS (ConocoPhillips, 2011b).

3.2. CarboCAT (carbonate cellular automata)

3.2.1. Numerical forward model formulation and model parameters

Run in MatlabR2016b, CarboCAT comprises a series of Matlab files (.m) that store different functions as ASCII files (.txt). The input parameters are defined by the user and are constant through the model run (Tables 1 and 2). Input parameters for CarboCAT comprise:

a) Model dimensions and cell size;
b) Total elapsed model time and duration of each time-step;
c) Subsidence rate;
d) Initial bathymetry of the model;
e) Number of producing carbonate factories, their distribution and production profiles;
f) Eustatic sea level.

The main controls on carbonate development, and the validity of different stratigraphic interpretations of seismic geometries in the Browse Basin (Rosleff-Soerensen et al., 2016; Belde et al., 2017; Van Tuyl et al., 2018), were investigated through a series of model runs described in Table 2. These model runs assumed different subsidence rates, and variable production rates, to replicate the geometry and stacking patterns observed on seismic data.

In order to evaluate the relative significance of each time-dependent

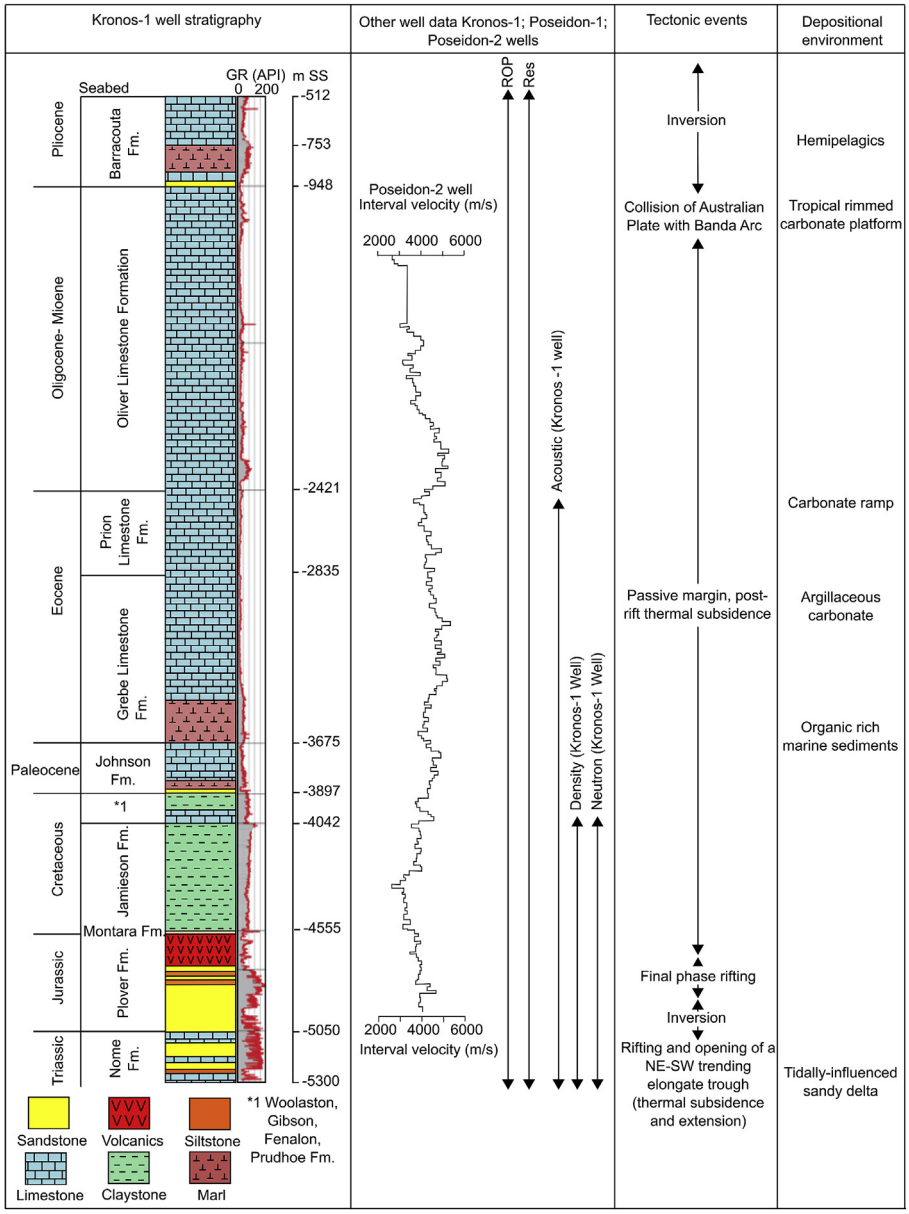

Fig. 2. Stratigraphic column of the Browse Basin showing the lithologies crossed by well Kronos-1, as well as available wireline data from the Kronos-1, Poseidon-1 and Poseidon-2 wells, including gamma-ray and interval velocity data. Well Kronos-1 shows the Miocene Formation to be 1475 m thick and comprising limestones. A sandstone unit is present over these Miocene carbonates, supporting the hypothesis of enhanced siliciclastic input in the Browse Basin during the demise of the carbonate build-ups studied here. Figure is modified from ConocoPhillips (2010, 2011a and 2011b).

process on carbonate evolution, only one of the tested parameters was changed each time within each model run (Table 2). The results from the multiple numerical models produced were then compared to the seismic dataset in terms of their geometry and stacking patterns. Qualitatively and quantitatively, the models that do not meet the interpreted data were considered as non-representative.

3.2.2. Initial conditions and input parameters

The input parameters used in the CarboCAT models are summarised in Table 1. The models aimed at simulating a carbonate sequence on a scale comparable to the Poseidon 3-D seismic volume. Whenever possible, the initial model conditions were based on the seismic interpretation in Van Tuyl et al. (2018) and this work, and data from the literature (e.g. Miller et al., 2005; Warrlich et al., 2008; Belde et al., 2017). One set of input parameters was kept constant in all CarboCAT models so as to reflect the initial modelling conditions (Table 1). These include model dimensions, cell size, model duration, initial bathymetry, initial water depth, eustatic sea level, carbonate production profiles and initial facies distribution. The second group contains the parameters (e.g. time-dependent processes) that are tested in each model run. These include subsidence rates, the percentage of produced sediment available for transport, and the effects of environmental deterioration (Table 2).

3.2.3. Numerical carbonate production

The current understanding of the Browse Basin favours a Miocene carbonate factory that was tropical and dominated by reef-building species (Rosleff-Soerensen et al., 2012, 2016; Howarth and Alves, 2016; Belde et al., 2017; Van Tuyl et al., 2018). Belde et al. (2017) and Van Tuyl et al. (2018) identified five seismic facies in the Browse Basin build-ups (Fig. 3). These comprise a pelagic facies, lower-slope and upper-reef facies, lagoonal facies and peri-reefal facies. To reflect these facies using the concepts of carbonate factory and carbonate production data in Bosscher and Schlager (1992), Warrlich et al. (2002, 2008) and

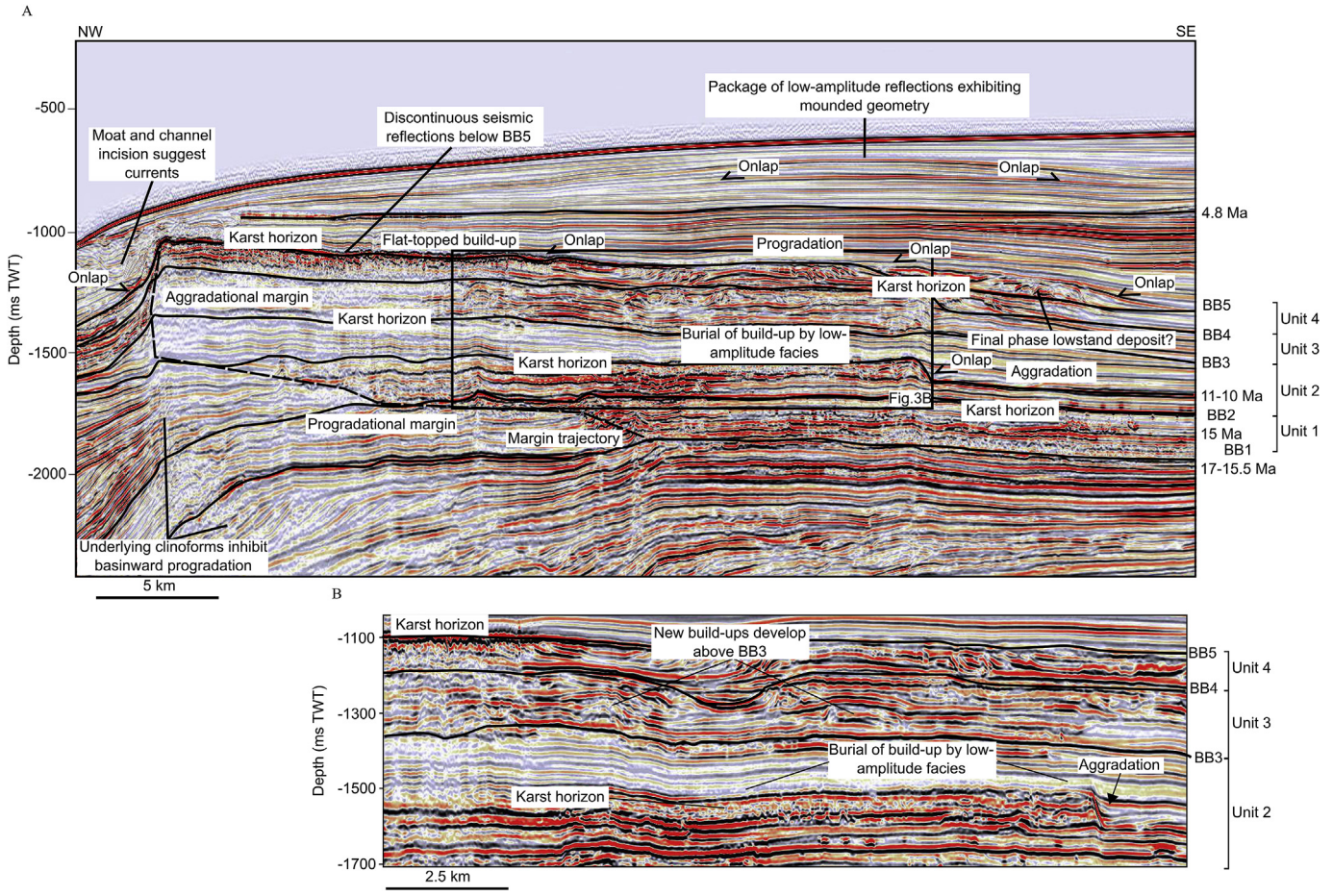

Fig. 3. Interpreted seismic profiles showing (A) a sequence-stratigraphic interpretation of the Miocene carbonate sequence. Five sequence boundaries subdivide the Miocene into four seismic stratigraphic units. Growth patterns show Unit 1 and the first part of Unit 2 to be progradational in nature, with accompanying karst horizons. Progradation is restricted by the antecedent topography imposed by the underlying Eocene-Oligocene carbonate ramp. The upper half of Unit 2 is characterised by aggradation, with carbonate build-ups being onlapped and buried by low-amplitude strata. (B) BB3 marks the top of the aggradational phase with the establishment of new build-ups and the progradation of the build-up to the southeast during the deposition of Unit 3. Progradation is accompanied by discontinuous reflections marking karst horizons. Unit 4 does not exhibit significant platform thickening, rather following an initial short-lived aggradational phase. The fine growth patterns indicate progradation, with sequence boundary BB5 revealing important karstification.

Burgess (2013), we simulated a tropical carbonate platform comprising three carbonate factories and one pelagic factory (Tables 1 and 2). The base euphotic zone was set at 40 m water depth, below which the pelagic factory was active. In order to consider the presence of a peri-reefal facies in the models, we assigned a facies transport algorithm to Factories 1, 2 and 3. These parameters were kept constant throughout

Table 1
Table summarising the input parameters kept constant throughout all model runs and the justifications behind their choice. Input values were derived from the literature, modern analogues and seismic interpretation, to constrain the models as accurately as possible.

Parameter	Value	Justification/source
Model duration	16.5 to 4.66 Ma (11.85 Ma)	The current literature dates build-up initiation between 17 Ma and 15.5 Ma above the Horizon C in Belde et al. (2017) and BB1 in this work. No absolute ages are available from wells (Fig. 2) for this horizon so 16.5 ± 1 Ma was chosen as a mid point to incorporate uncertainty. Demise is proposed to occur between 10 and 6 Ma with drowning complete by 4.8 Ma (Belde et al., 2017). Consequently, all models run through to 4.66 Ma (Pliocene).
Time steps	3 kyrs	Trade off between resolution and model run time (Antonatos, 2018)
Cell size	500 m	Trade off between resolution and model run time
Model size	50 km × 25 km	Reflects the size of the Poseidon 3-D dataset
Initial bathymetry	BB1	Seismic interpretation and depth conversion of base Miocene (ConocoPhillips, 2012)
Production rates	Reef facies: 4500 m/Ma Interior 1 and 2: 3500 m/Ma Pelagic: 50 m/Ma	Modern analogues (Bosscher and Schlager, 1992; Warrlich et al., 2002, 2008)
Initial facies distribution	Random	Reflects reef-building organisms carried by currents
Initial water depth	1 m	BB0 interpreted as karst horizon. A depth of 1 m reflects re-flooding.
Wave height	1 m	Mean wave heights in the Browse Basin (CALENERGY Resources (Australia) Ltd., 2013)
Initial rate of degradation	50%	Warrlich et al. (2008)
Critical slope angle	40° for Factory 1, 20° for Factories 2 and 3	Kenter (1990)

Table 2
Table summarising the variable parameters used in the CarboCAT numerical modelling in this work. Nine (9) models were run to test the influence of different time-variable processes on the Miocene carbonate system over a period of 11.84 Ma, based on the dating of the Miocene sequence in Belde et al. (2017) and Van Tuyl et al. (2018).

Model Run	Model run time and time-steps	Test	Subsidence rate	Initial topography	Eustatic Sea level	Production rates (Warrlich et al., 2008)	Percentage of produced material available for transport (degradation)
1	Model run time 16.5 Ma to 4.66 Ma Model time-steps: 3 kyrs	Current literature	Subsidence rate from 16.5 Ma to 4.66 Ma based on data in Belde et al. (2017)	Seismic interpretation of BB1 (Base Miocene), which correlates with the depth-converted intra-Oligocene horizon in ConocoPhilips (2012)	Miller et al. (2005)	Reef: 4500 m/Ma^{-1} Lagoon 1: 3500 m/Ma^{-1} Lagoon 2: 3500 m/Ma^{-1} Pelagic: 50 m/Ma^{-1}	Reef: 50% Lagoon 1: 10% Lagoon 2: 10% Pelagic: 0% (Warrlich et al., 2008)
2	As above	Current literature with a reduction in transported carbonate sediment	As above	As above	As above	As above	Reef: 25% Lagoon 1: 10% Lagoon 2: 10% Pelagic: 0%
3	As above	Current literature hypothesis considering and differences in transported material	As above	As above	As above	As above	Reef: 35% Lagoon 1: 10% Lagoon 2: 10% Pelagic: 0%
4	As above	Linear subsidence rate	132 m/Ma based on a thickness-age calculation from seismic line	As above	As above	As above	As above
5	As above	Pulsed subsidence	Variable through time	As above	As above	As above	As above
6	As above	Progressively increasing subsidence	Exponentially increasing sea-level curve from 10 to 1061 m/Ma	As above	No sea-level change	As above	Reef: 35% Lagoon 1: 10% Lagoon 2: 10% Pelagic: 0%
7	As above	Moderate environmental deterioration	Subsidence rate from 16.5 Ma to 4.66 Ma based on data in Belde et al. (2017)	Seismic interpretation of BB1 (Base Miocene), which correlates with the depth-converted intra-Oligocene horizon in ConocoPhilips (2012)	Miller et al. (2005)	25% decrease in production rate from 10 Ma	Reef: 35% Lagoon 1: 10% Lagoon 2: 10% Pelagic: 0%
8	As above	Significant environmental deterioration	As above	As above	As above	50% decrease in production rate from 10 Ma	As above
9	As above	Very significant environmental deterioration	As above	As above	As above	75% decrease in production rate from 10 Ma	As above

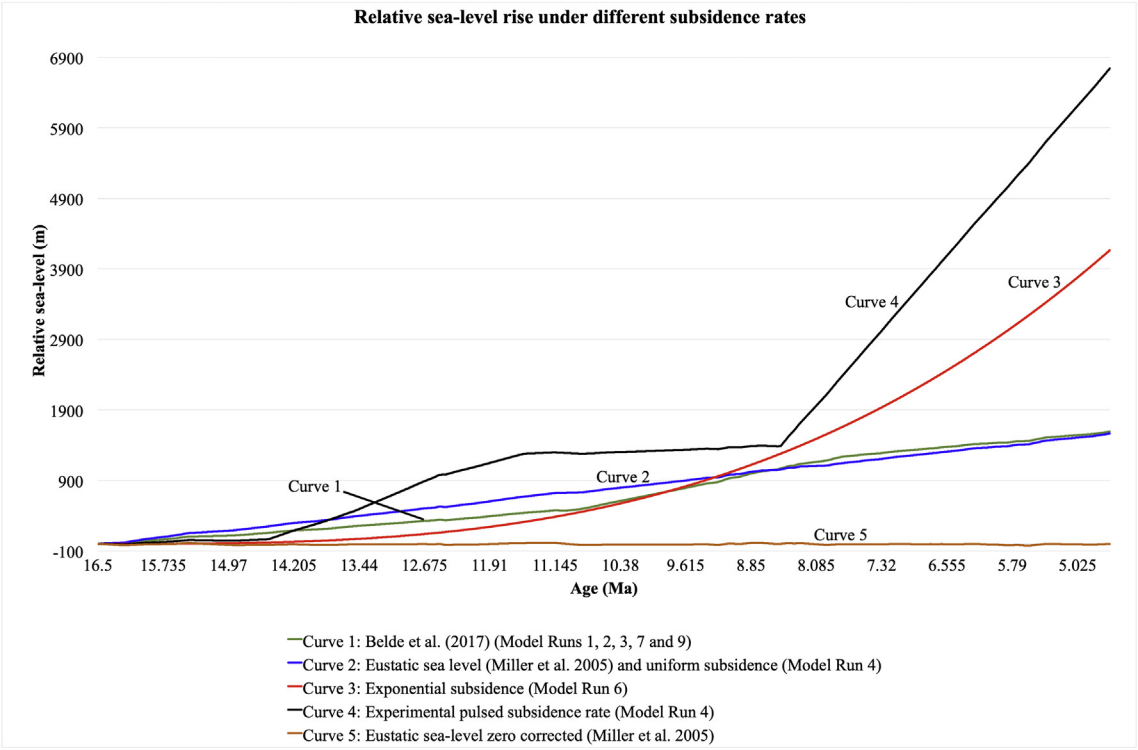

Fig. 4. Graph showing the relative sea-level curves used in the model runs. Curve 1 reflects the combination of the Miller et al. (2005) eustatic sea-level curve and the subsidence rates proposed for the northern Browse Basin by Belde et al. (2017). Curve 2 marks the combined effects of the Miller et al. (2005) eustatic sea-level curve and a uniform subsidence rate of 132 m/Ma. Curve 3 represents the effects of a progressively increasing subsidence rate, starting at the 132 m/Ma subsidence rate proposed for the Browse Basin and increasing every year to a maximum of 622 m/Ma. Curve 4 represents the sum of the Miller et al. (2005) eustatic sea-level curve and an experimental subsidence curve representing alternative pulses of fast and slow subsidence rates. Curve 5 represents the Miller et al. (2005) eustatic sea-level curve.

all model runs (Table 1).

Factory 1 simulates a very shallow euphotic type, restricted to shallow waters, with maximum production rates recorded up to a depth of 10 m. It comprises carbonate-producing organisms that require high light levels, but produce carbonate at fast rates (Burgess, 2013). Factory 1 represents the reef framework that occupies shallow high-energy environments and is wave resistant.

Factory 2 reflects a second euphotic type restricted to shallow waters, with maximum production rates recorded up to a depth of 10 m. It is chiefly composed of lagoonal patch-reef facies (Lagoon 1), and represents organisms with a slower production rate than Factory 1.

Factory 3 represents a third euphotic type restricted to shallow waters, with maximum production rates recorded up to a depth of 10 m. It simulates organisms producing carbonate at a slow rate (Burgess, 2013). It represents low-energy lagoonal facies (Lagoon 2), and is less resistant to wave energy than Factories 1 and 2.

Factory 4 replicates a pelagic factory producing carbonates at a slower rate than all other factories considered, and only below a depth of 40 m. This facies represents pelagic environments and is not resistant to wave energy.

The application of wave energy to the model runs was based on seismic interpretation by Howarth and Alves (2016) and Van Tuyl et al. (2018), which identified the northwest margins of carbonate build-ups as facing into the waves, while southeast leeward margins are sheltered (Fig. 3). As specified above, each factory was assigned a range of wave energies it could tolerate, outside of which production ceased. A wave height of 1 m was assigned to the models to simulate fair-weather conditions based on mean wave heights recorded in the Browse Basin during the Offshore Drilling Campaign WA-424-P (CALENERGY Resources (Australia) LTD, 2013) (Table 1).

3.2.4. Carbonate factory rules

Simple rules representing an approximation of the principles of spatial carbonate-factory competition, resource availability, and the resulting minimum and maximum thresholds of population size required for survival, were defined in the cellular automata algorithm and applied to the model runs. The aim was to determine the state of each cell at the next iteration or time step (Burgess, 2013). For a carbonate factory to survive within an individual cell, or to trigger the colonisation of an adjacent cell, one adjoining cell needs to host the same factory. However, these values are poorly constrained due to the sparse data available in the literature characterising the degree of spatial competition among carbonate factories (Burgess, 2013). When cells have been exposed and later re-submerged, the cell is either occupied by the last carbonate factory, or left empty.

3.2.5. Subsidence

In CarboCAT, users can define subsidence rates for the whole model, or for individual cells (Table 2). The current literature for the northern Browse Basin proposes an average subsidence rate of 125 m/Ma for the duration of the interpreted Miocene carbonate sequence (see Belde et al., 2017). The southern part of the Browse Basin records an average subsidence rate of 64 m/Ma. In the study area, the Miocene sequence has a thickness of 1475 m, and was deposited between ~16.5 Ma and the end of the Miocene (5.33 Ma), i.e. it is slightly younger that the sequence modelled in Belde et al. (2017). The carbonate sequence considered in this work reflects an average subsidence rate of 132 m/Ma.

To test the role of accelerated subsidence in Miocene carbonate evolution, we ran a series of models with different subsidence profiles based on the current literature from the Browse Basin to replicate the interpreted seismic volume. Model Runs 1 to 3 tested the subsidence

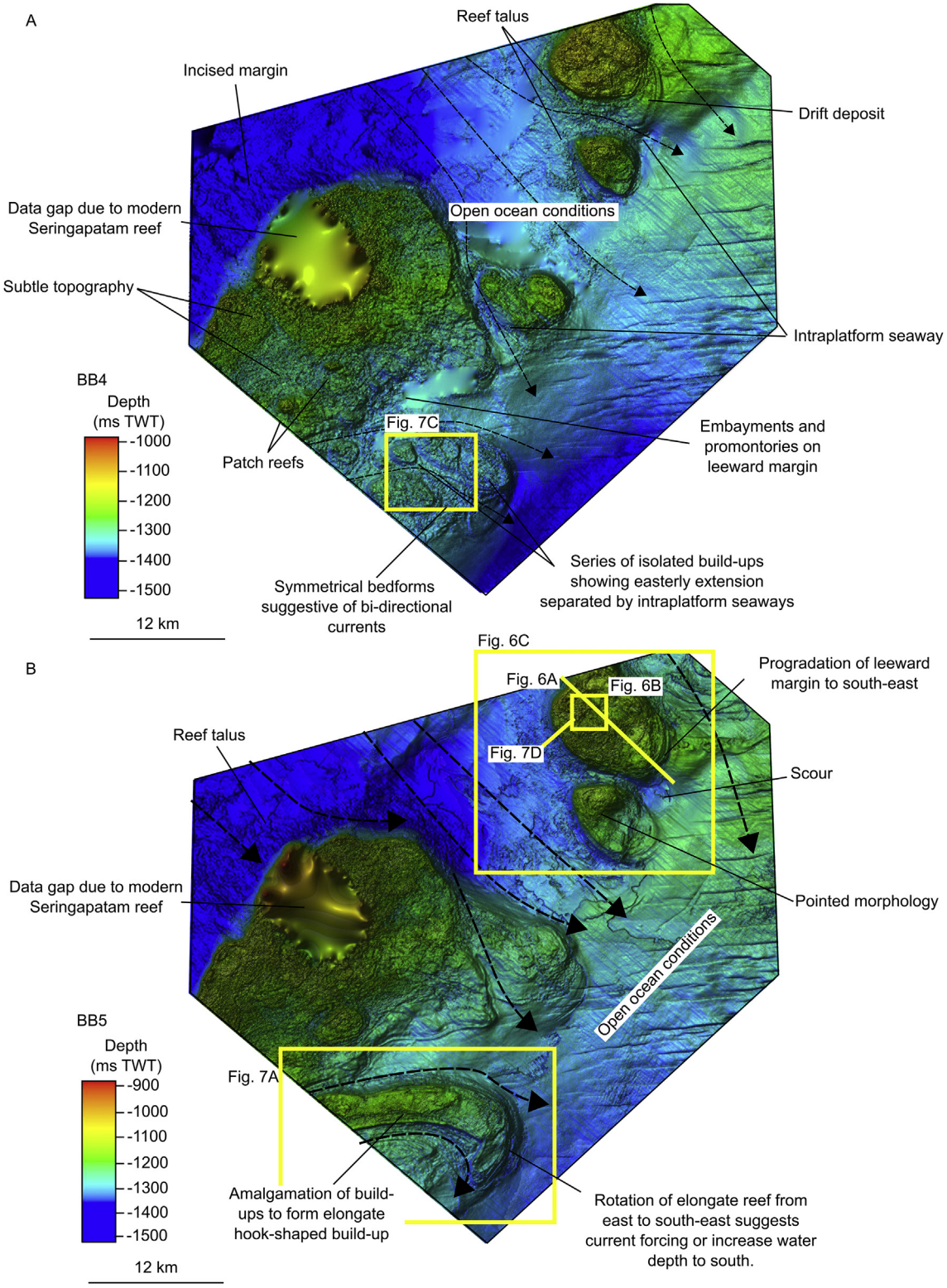

Fig. 5. (A) Two-way time (TWT) structure map showing BB4 and the relative locations of Figs. 6 and 7. (B) TWT structure map showing horizon BB5 and the relative locations of Figs. 6 and 7. Fig. 5A and B shows the morphological evolution of isolated carbonate build-ups during the last phases of Miocene reef growth. Both figures show features that are typical of a current-driven depositional system with intraplatform seaways, scours and sand-wave bedforms.

profile for the northern Browse Basin proposed in Belde et al. (2017). Model run 4 tested the impact of a linear subsidence rate (average 132 m/Ma), applied to the Miller et al. (2005) eustatic sea-level curve, in order to document the effect of this latter on carbonate-growth patterns (Table 2 and Fig. 4).

Model Run 5 tested the effects of an experimental subsidence rate comprising pulses of fast and slow subsidence applied to the Miller et al. (2005) sea-level curve (Table 2 and Fig. 4). This was done as an iterative process comprising 22 model runs, starting with the base subsidence profile of Belde et al. (2017). Each model run was split into

1 Ma blocks, and subsidence rates were changed following the ranges defined for the North West Shelf (Belde et al., 2017), and the maximum subsidence rates for margins associated with subduction (Galewsky et al., 1996) (Table 2).

Model Run 6 tested the effects of a progressively increasing subsidence rate, starting at the 10 m/Ma subsidence rate proposed for the Browse Basin, and increasing every year to a maximum of 1061 m/Ma. This latter value is more than three times the present-day subsidence rate documented just north of the Scott Reef (Hengesh et al., 2010) (Table 2).

Model Runs 7 to 9 used the subsidence profile of Belde et al. (2017) for the northern Browse Basin (Table 2).

3.2.6. Eustatic sea level

CarboCAT (Burgess, 2013) allows users to define a sinusoidal sea-level curve for the modelling, or import a sea-level curve from an external file (Tables 1 and 2 and Fig. 4). Numerous reconstructions of Miocene eustatic sea level have been published (e.g. Haq et al., 1987; Vail and Hardenbol, 1979; Miller et al., 2005; John et al., 2011; Tesch et al., 2018). In this study, we use the Miller et al. (2005) sea-level curve spanning the entire Miocene and providing third to fourth order sea-level cycle resolution. This sea-level curve is derived from backstepping data from 16.5 Ma to 7 Ma (Van Sickel et al., 2004), and from 7 Ma to 4.6 Ma based on $\delta^{18}O$ values from Miller et al. (1987). This same sea-level curve was applied by Saqab and Bourget (2016) to interpret Miocene reef growth in the northern Bonaparte Basin, North West Australia. We created a.txt file of the Miller et al. (2005) sea-level curve in Microsoft Excel with the same number of iterations as the model, and imported it into CarboCAT.

4. Seismic interpretation of Miocene growth patterns

4.1. BB1 to BB2: progradation (Unit 1)

Following its initiation above BB1, the carbonate sequence comprises sigmoidal seismic reflections that are typical of progradational strata (Fig. 3). This progradational stage moved the build-up margin 18 km to the northwest towards the break in slope created by the underlying clinoforms on the carbonate ramp (Fig. 3). Progradation does not occur beyond the break in slope. This progradational sequence is capped by sequence boundary BB1 (Fig. 3).

4.2. BB2 to BB3: aggradation (Unit 2)

Above BB2, the sequence is characterised by seismic reflections with build-in and build-up geometries (Fig. 3). The southeast margins of build-ups are forced to retrograde by up to 6 km, while the northwest margins remain fixed and become aggradational (Fig. 3). This develops a prominent margin morphology, which is onlapped by low-amplitude, uniform seismic reflections from the northwest and southeast (Fig. 3). The culmination of this first aggradational phase is marked by sequence boundary BB3, which is characterised by high variance and circular features that correlate with discontinuous seismic reflections on vertical seismic profiles (Fig. 3).

4.3. BB3 to BB4: establishment of new build-ups (Unit 3)

Above BB3, new carbonate build-ups were established southeast of surviving build-ups (Fig. 3). Initially aggradational (Figs. 3, 5A and 6 and 7), the build-ups become progradational to the southeast, resulting in the amalgamation of carbonate edifices that were initially separated (Fig. 7A and B). Following this stage, another phase of backstepping occurs. Once again, this backstepping is concentrated on the southeast margins of build-ups and caused their retreat 6 km to the northwest (Fig. 6A).

4.4. BB4 to BB5: progradation and karstification (Unit 4)

Following the aggradational phase represented by Unit 3, another phase of progradation is observed above BB4 (Figs. 3 and 5B). At this stage, sigmoid to sigmoid-oblique seismic reflections expand the leeward margin of build-ups by 2 km to the southeast (Fig. 6A). The final build-up horizon is characterised by its high variance and circular to dendritic features that typically stem from topographic highs (Fig. 6B). Build-ups exhibit flat-topped topography that is up to 10 km wide (Fig. 6A). The very top of Unit 4 exhibits some subtle topography, but there are no prominent aggradational structures (Fig. 6A and C).

4.5. Appearance of sediment drifts between BB3 to BB5

The final carbonate build-ups are onlapped and buried by low to moderate amplitude, often wavy, seismic packages (Figs. 3, 6A and 8A, 8B and 9). These packages show mounded geometries and generate positive topography. Some of these features exceed 24 km in diameter and thin laterally wherever they downlap onto the underlying surface (Fig. 8A and B). The orientation of these features is northwest-southeast, perpendicular to the shelf margin. Onlapping strata are observed where these features interact with isolated carbonate build-ups, with V-shaped geometries often occurring at the intersection of these deposits with the carbonate build-up margin, marking important incision (Fig. 8). A number of these packages completely drape and enclose the carbonate build-ups (Fig. 7A), while others exhibit stacked geometries proximal to build-up margins (Fig. 7B). Within these stacked sequences, downlaping and onlapping reflections are observed between different packages (Fig. 8A and B and 9). Seismic reflections are locally truncated and V-shaped negative topography is observed where individual seismic packages overlie one another (Fig. 9). The bases of individual packages exhibit angular geometries (Fig. 9).

The initial deposition of the mounded packages is coincident with the appearance of northwest-striking, symmetrical to asymmetrical sand waves, and scour features associated with intraplatform seaways (Figs. 6C and 7C). Spatial variations in build-up morphology are also observed at this time, including: 1) long-axis rotations of build-ups from a northwest-southeast to a more north-northwest to south-southeast orientation, before returning to a clear northwest strike (Fig. 6C); 2) 'Bent-elbow' morphologies characterised on one build-up margin by clinoforms with a sigmoidal geometry, and on the other build-up margin by limited progradation and a more continuous seismic character (Fig. 7A and B); 3) Pointed geometries to the northwest (Figs. 6C, 7A) and 4) evidence for proximal build-ups influencing each other's margins (Fig. 6C).

4.6. Summary of seismic interpretation

Seismic interpretation identifies a Miocene carbonate sequence that is 1475 m thick and progrades 18 km. From its initiation to its demise, five sequence boundaries were formed. The underlying topography restricts progradation to the northwest. A major aggradational event occurs after the initial progradation phase. Thereafter, alternating aggradation and progradation characterises the final stages of carbonate production. During their final stages, the carbonate build-ups are onlapped and buried by mound-shaped seismic packages.

5. Stratigraphic forward modelling (CarboCAT)

5.1. Regional evolution

All model runs where computed using the input parameters in Tables 1 and 2, and Fig. 4, to model the effects of different time variable controls on carbonate evolution.

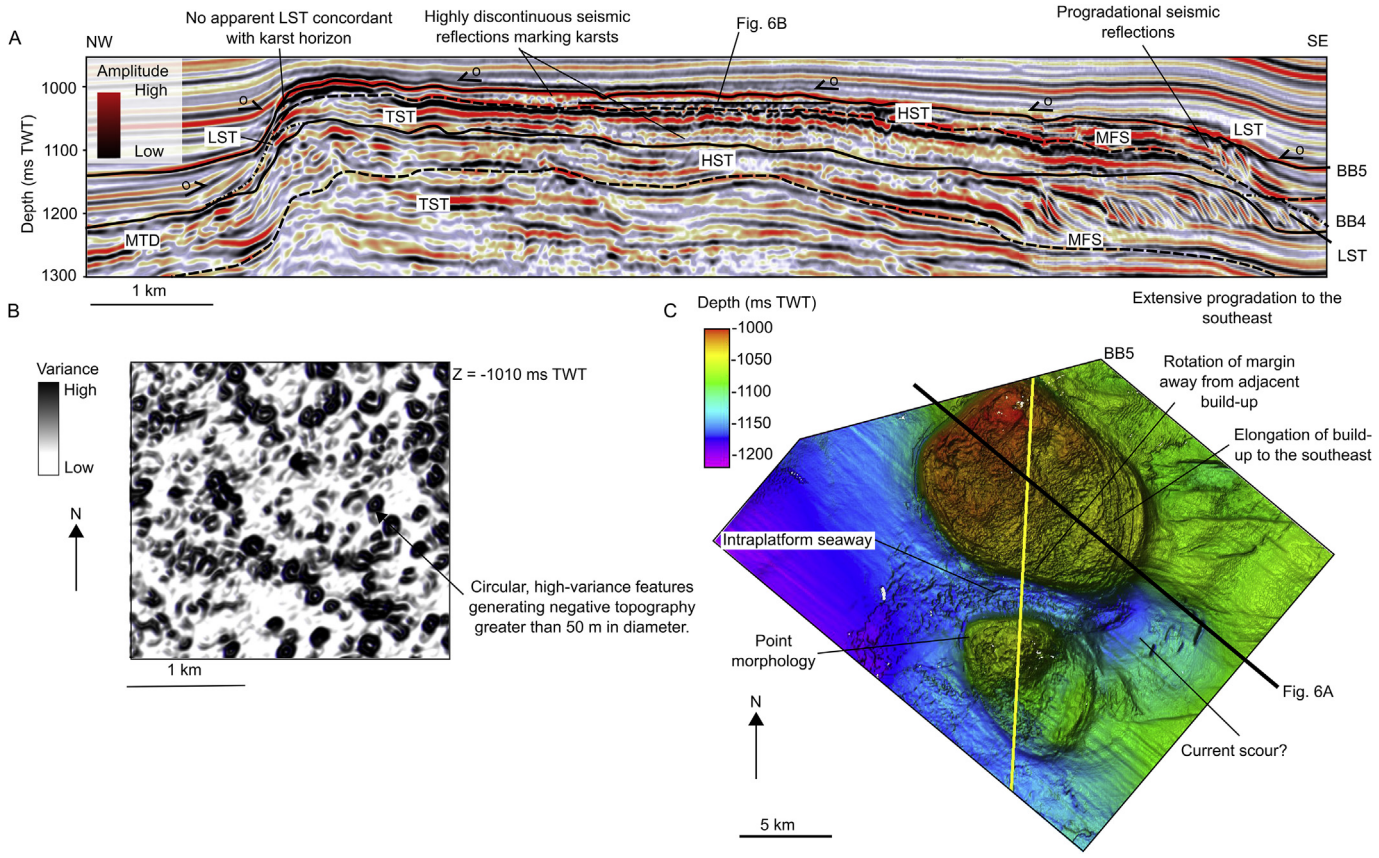

Fig. 6. (A) Interpreted seismic profile showing the final stages of carbonate build-up growth in the Browse Basin. The final growth phases show an initial transgressive aggradational phase switching to progradational and extending the margin 5 km to the southeast, as marked at its edge by a lowstand deposit. Thereafter, a short-lived transgressive phase overlies BB4 and forces margin retreat. The final phase of growth is characterised by progradation to the southeast and evidence of a lowstand deposit. BB5 is characterised by highly discontinuous seismic reflections suggestive of karsts, with the topmost seismic reflection showing some small subtle topography, but generally a flat top with no aggradational phase. (B) Variance slice through BB5 showing this sequence boundary as comprising high-variance circular to dendritic features with diameters of 60 m. These correlate with highly discontinuous seismic reflections and are interpreted as karsts. (C) Two-way time (TWT) structure map of BB5 revealing northeast-southwest elongation of final phase carbonate build-ups. An intraplatform seaway is observed between the two build-ups, with a topographic depression observed where the intraplatform seaway exits the two build-ups. Carbonate build-up margins show evidence for rotation away from one another due to currents.

5.1.1. Model run 1: variable subsidence rates in Belde et al. (2017)

In Model Run 1, marked progradation (~8.5 km) occurs from 16.5 to 15.4 Ma once the margin is established (Fig. 10 and Table 3). Thereafter, aggradation thickens the build-up by 60 m until 14.85 Ma. Subsequent progradation of 5.5 km occurs until 12.3 Ma, when the interior is sub-aerially exposed. Re-submergence at 12.0 Ma sees strata progradation approaching 8 km until 8.16 Ma. Initially this progradation is slow, but becomes pronounced after 10.46 Ma, moving the margin beyond the antecedent break in slope. Thereafter, the build-up progrades 2 km and aggrades 406 m until the end of the model run at 4.64 Ma (Fig. 10). Carbonate production does not terminate by the end of the Miocene (5.33 Ma).

5.1.2. Model run 2: variable subsidence rates in Belde et al. (2017) with 25% of produced facies available for transport

In Model Run 2, the overall geometry is progradational (7 km) towards the break in slope following the onset of carbonate deposition (Fig. 11 and Table 3). At 13.5 Ma, carbonate production shuts off and the build-ups are drowned to reach a total thickness of 266 m (Fig. 11).

5.1.3. Model run 3: variable subsidence rates in Belde et al. (2017) with 35% of produced facies available for transport

Model Run 3 shows that, once established, the margin progrades 5.5 km until 15.4 Ma, thickening by 133 m (Fig. 12 and Table 3). A pronounced aggradational phase thickens the build-up by 333 m until 12.5 Ma, accompanying 4.5 km of progradation. Sub-aerial exposure of the platform interior until 12.2 Ma is followed by its re-submergence, a progradation of ~2 km and an aggradation of 133 m until 10.5 Ma. The margin then progrades 4.5 km basinwards and aggrades 333 m by 8.5 Ma (Fig. 12). Pronounced aggradation of 687 m, and progradation of 2.5 km, characterise the sequence until the end of the model run (4.64 Ma). Carbonate production does not terminate by the end of the Miocene (5.33 Ma).

5.1.4. Model run 4: linear subsidence rate with 35% of produced facies available for transport

In Model Run 4, the margin progrades 7 km and aggrades 125 m by 15.3 Ma (Fig. 13 and Table 3). Thereafter, an aggradation of 357 m and progradation of 4.5 km occur until 12.3 Ma. Subsequent sub-aerial exposure of the platform interior occurs until 12.2 Ma. Following re-flooding, an aggradation of 1 km and progradation of 5.5 km occur on the platform until the end of the model run (Fig. 13). Carbonate production does not terminate by the end of the Miocene (5.33 Ma).

5.1.5. Model run 5: pulsed subsidence with 35% of produced facies available for transport

In Model Run 5, the interior is sub-aerially exposed at 16.4 Ma (Fig. 14 and Table 3). Thereafter, a progradation of 6 km and aggradation of 71 m occur after 16.1 Ma. A second phase of sub-aerial exposure, from 15.4 Ma to 14.7 Ma, is followed by 12 km of

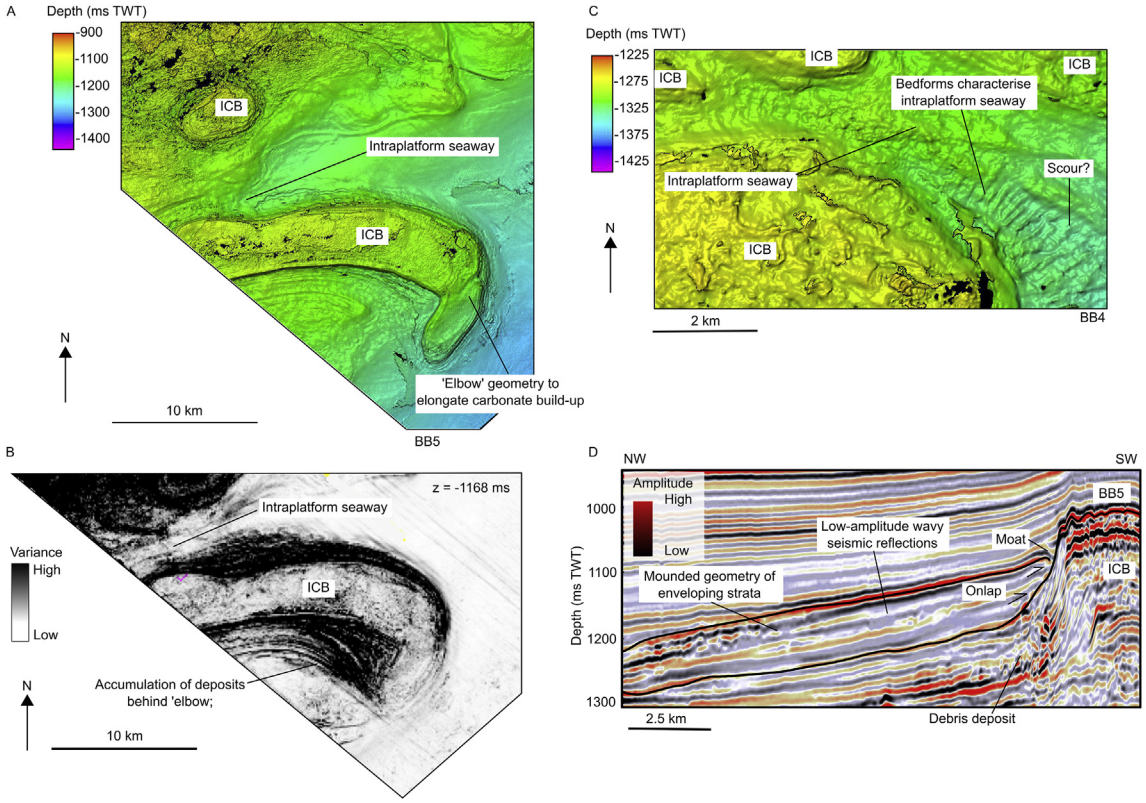

Fig. 7. (A) Two-way time (TWT) structure map of BB4 showing an elongated E-W striking carbonate build-up with an 'elbow' geometry, marked on its northern margin by an intraplatform seaway separating it from a larger build-up to the north. Elongation and the elbow geometry suggest that currents controlled its shape. (B) Variance time-slice through the 'elbow-shaped' reef in Fig. 7A showing high-variance clinoforms behind the elbow. This character suggests progradation or lowstand deposits. The absence of these clinoform geometries on the northern margin suggests the elbow protected its southern margin from currents. (C) TWT structure map showing evidence for bedform structures within an intraplatform seaway developed between a number of carbonate build-ups. This indicates that high-energy currents were active. (D) Interpreted seismic profile showing a moat structure formed where drowning strata onlap a carbonate build-up. This suggests that currents were wrapped around the carbonate build-up and removed material from the slope.

progradation and 1214 m of aggradation until 10.8 Ma (Fig. 14). At 13 Ma, the platform interior backsteps and is locally drowned. Subsequently, carbonate build-ups show progradation in the order of 10 km. A further sub-aerial exposure event between 10.8 and 10.2 Ma is followed by aggradation of 178 m and progradation of 500 m until 8.1 Ma (Fig. 14). Three sub-aerial exposure events occur at 9.17 Ma, 8.88 Ma and 8.59 Ma, before production ceases at 8.1 Ma (Fig. 14).

5.1.6. Model run 6: progressively increasing subsidence rates

In Model Run 6, the margin progrades 18 km and aggrades by 4222 m over the entire time-span of the model, becoming increasingly aggradational (Fig. 15 and Table 3). At 9 Ma, the larger build-up is split into isolated pinnacle reefs, which are purely aggradational until the end of the model run. Carbonate production does not terminate by the end of the Miocene (5.33 Ma) (Fig. 15).

5.1.7. Model run 7: production suppression (25%)

In Model Run 7, the margin progrades 5.5 km and aggrades 133 m between 16.5 Ma and 15.4 Ma (Fig. 16 and Table 3). Thereafter, the margin aggrades 333 m and progrades 4.5 km until 12.5 Ma, anticipating sub-aerial exposure. From 12.2 Ma to 10.5 Ma, the build-up is re-submerged, progrades 2 km and aggrades 133 m, before prograding 4.5 km and aggrading 333 m until 8.5 Ma (Fig. 16). From 8.5 Ma until the end of the model run (4.6 Ma), the margin progrades 2.5 km and aggrades 687 m. Carbonate production does not terminate by the end of the Miocene (5.33 Ma) (Fig. 16).

5.1.8. Model run 8: production suppression (50%)

In Model Run 8, the margin progrades 5.5 km and aggrades by 133 m until 15.4 Ma (Fig. 17 and Table 3). Thereafter, the margin progrades 4.5 km and aggrades 333 m until 12.5 Ma, before being sub-aerially exposed. The re-submergence of the margin after 12.2 Ma is marked by 2 km of progradation and 133 m of aggradation until 10.5 Ma. Thereafter, the margin progrades 3 km and aggrades 333 m until 9.1 Ma, becoming progressively more aggradational (Fig. 17). From 9.1 Ma until the end of the model run (4.6 Ma), the margin progrades 1 km and aggrades 833 m. Carbonate production does not terminate by the end of the Miocene (5.33 Ma) but becomes more isolated from 8.7 Ma onwards, with parts of the platform interior becoming buried by pelagic facies (Fig. 17).

5.1.9. Model run 9: production suppression (75%)

In Model Run 9, the margin progrades 5.5 km and aggrades 133 m until 15.4 Ma (Fig. 18 and Table 3). Thereafter, the margin progrades 4.5 km and aggrades 333 m until 12.5 Ma. Sub-aerial exposure occurs until 12.2 Ma, with subsequent re-submergence leading to 2 km of progradation, and an aggradation of 166 m until 10.9 Ma. Subsequently, the margin aggrades by 500 m as isolated pinnacles, with no progradation (Fig. 18). Carbonate production is terminated by the end of the Miocene (8.7 Ma).

5.2. Summary and comparison of stratigraphic forward modelling (CarboCAT) to seismic interpretation

Model Runs 1 to 3 show that the amount of sediment produced at the base of slope influences the ability of carbonate factories to respond to sea-level rise (Table 3). Model Runs 3 and 4 replicate the currently accepted evolution models for the Browse Basin (e.g. Belde et al., 2017,

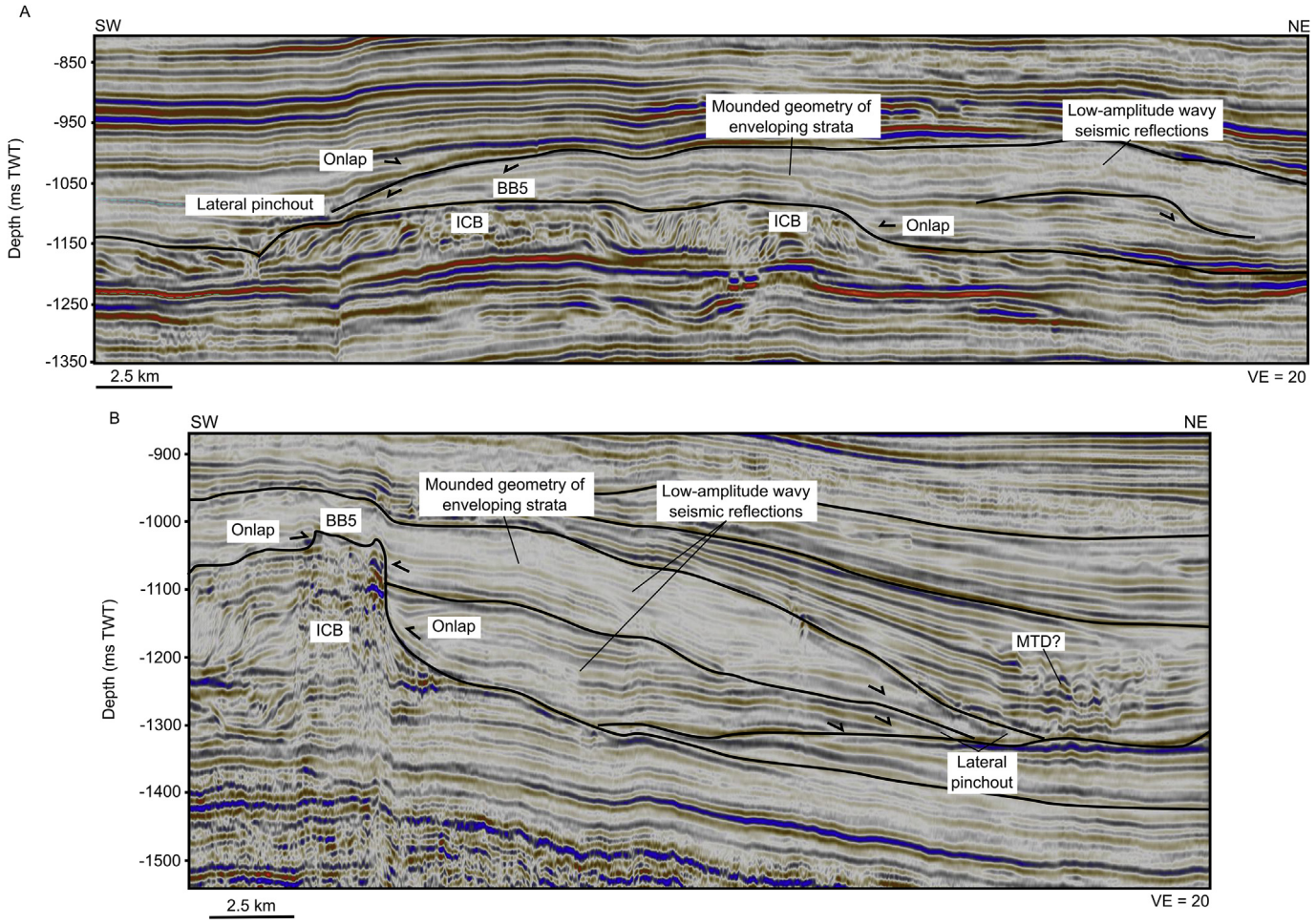

Fig. 8. (A) Interpreted seismic profile br98_156 showing a package of low-amplitude, wavy seismic reflections with a mounded geometry and lateral pinch-outs burying sequence boundary BB5 (top of the studied Miocene carbonate build-ups). The mounded package shows onlapping relationships and resembles sediment drifts. (B) Interpreted seismic profile hbr1998b-35 showing a series of packages with low-amplitude, wavy seismic reflections onlapping the final phase of carbonate build-ups. The seismic data shows these packages to stack against the carbonate build-up to bury it.

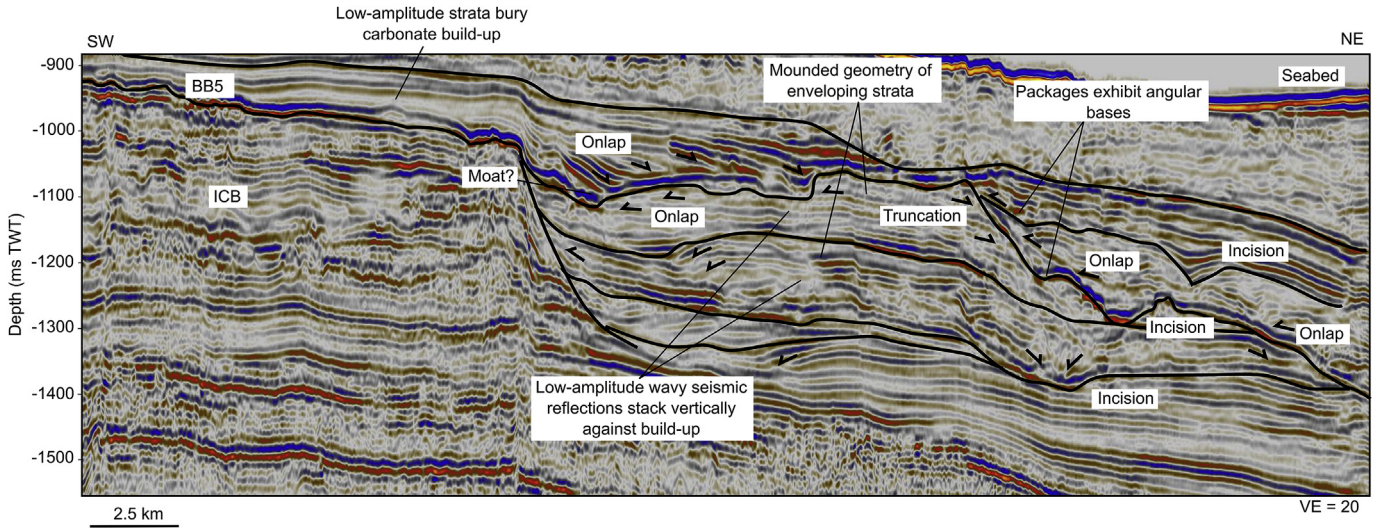

Fig. 9. Interpreted seismic profile br98_160 showing a series of stacked packages of mounded seismic reflections with onlapping and truncated geometries. V-shaped negative topography is observed at the margin of the carbonate build-up and within low-to moderate-amplitude wavy packages, suggesting erosion due to currents or channels. The seismic profile indicates that during the final stages of carbonate production, build-up topography was influenced by the deposition of these packages.

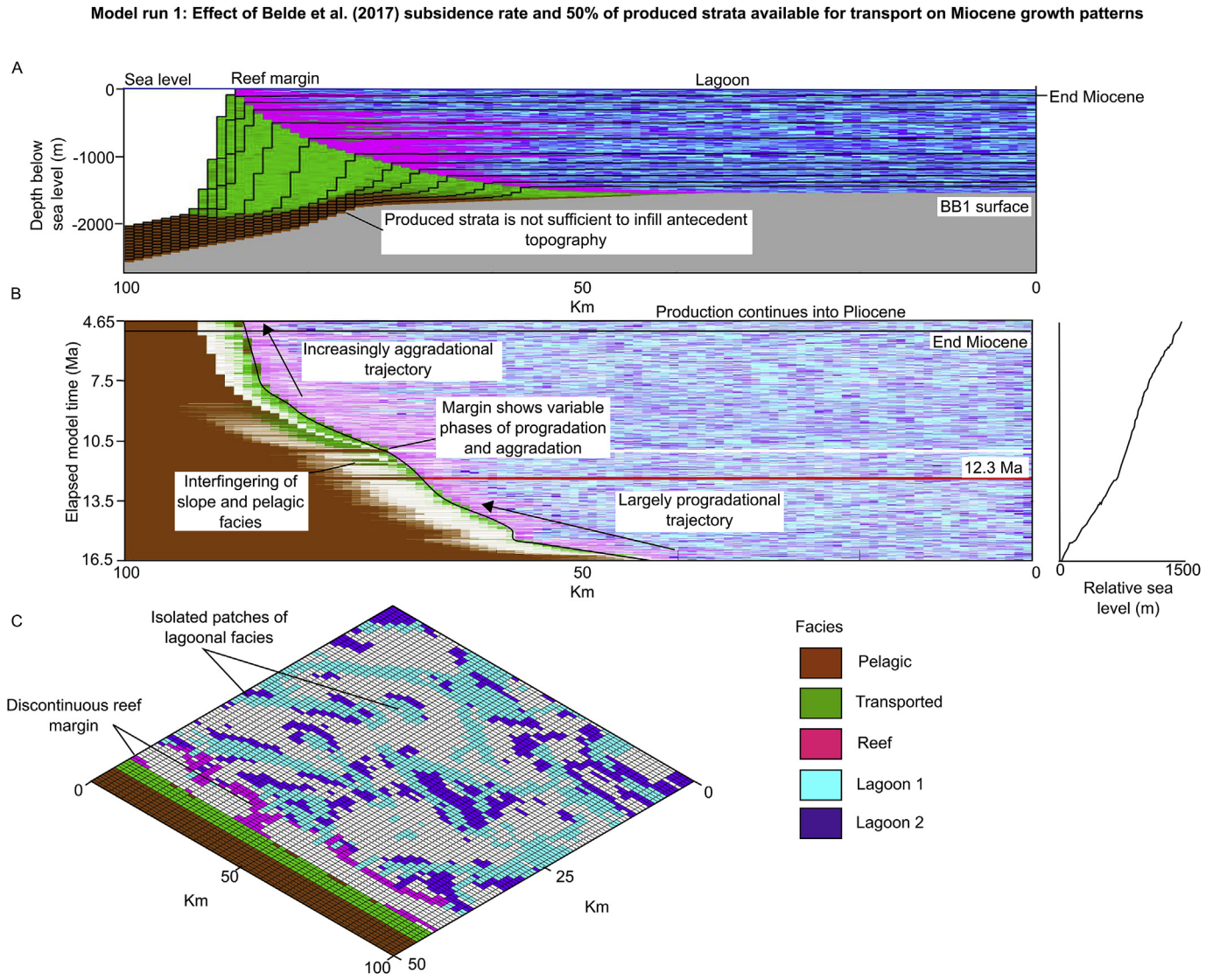

Fig. 10. CarboCAT Model Run 1 showing the effects the Belde et al. (2017) variable subsidence profile, combined with the Miller et al. (2005) sea-level curve and 50% of produced facies available for transport (see Warrlich et al., 2008), on the growth patterns of the Miocene carbonate sequence. The model shows an initial progradational sequence that transitions to an aggradational build-up. The pre-existing topography is partially filled by transported facies permitting sediment progradation beyond the break in slope. One sequence boundary is observed at 12.3 Ma. The carbonate sequence is characterised by a reef margin backed by a lagoon. Relative sea-level rise is not enough to drown the carbonate sequence by the end of the Miocene.

but are insufficient to create equivalent growth patterns and sequence boundaries to our seismic interpretation. Instead, Model Run 5 generates the best comparison among carbonate growth patterns, sequence boundaries and the geometries interpreted in the Poseidon-1 seismic volume. Model Runs 5 and 6 generate comparable geometries, but build-up thicknesses are greater than those interpreted on seismic data, a character revealing that subsidence rates in excess of 1100 m/Ma are required to drown the carbonate factories at full production rates (Model Run 6). Model Runs 7 to 9 reveal suppressed carbonate production associated with environmental deterioration, a factor making the carbonate factories susceptible to drowning. Models 7 to 9 generated the geometries interpreted on seismic data under the published eustatic sea-level and subsidence rates (Miller et al., 2005; Belde et al., 2017).

6. Discussion

6.1. Relative significance of subsidence vs. eustatic sea level on Miocene carbonate evolution

Numerical modelling aimed at identifying the key controls on the large scale geometry of the interpreted carbonate sequence. The results of this modelling are summarised in Table 3 and discussed below.

6.1.1. Eustatic sea level

Model runs 1 to 9 show that the eustatic sea-level oscillations from Miller et al. (2005) are of insufficient amplitude (< 40 m) and time span (< 1 Ma) to generate major growth patterns such as the aggradational phase in Unit 2 (Figs. 3 and 6). Significantly, eustatic sea-level fall was only able to create one sequence boundary under the proposed subsidence rates of Belde et al. (2017), when compared to the four (4) sequence boundaries interpreted on seismic data above BB1 (Van Tuyl et al., 2018) (Figs. 10, 12 and 13 and Table 3).

This latter caveat in Model Runs 1 to 9 may reflect: a) the relative

Table 3
Table summarising the outputs of numerical modelling compared to the interpreted seismic data. The published models in the literature do not generate a best-fit to the Browse Basin carbonate sequence. Instead, a pulsed subsidence model generates the most comparable geometries to the seismic data. However, this requires episodic subsidence on magnitudes far greater than proposed for the North West Shelf and suggests that the Miocene carbonate sequence was drowned before the end of the Miocene. The model results show that build-up demise is promoted more readily under the proposed Miocene subsidence rates and eustatic sea level by suppressing carbonate production, rather than by accelerating subsidence.

		Thickness at the end of the Miocene (km)	Total progradation (km)	No. of sequence boundaries	Sequence boundaries (Ma)	Demise (Ma)	Margin length (km)	Length of platform interior (km)	Facies distribution	Type	% Match	Figure
Seismic line		1475	18	5	16.5; 15; 11-10; 2 between 10 and 5.3	By 5.3	0.8	39	Initial barrier reef with reef margin backed by lagoonal area. Transitioned to isolated build-up morphology with reef margin backed by lagoons separated by suggested pelagic facies.	Rimmed platform	n/a	9
Model Run	1	1475	21	1	12.3	After 4.64	8	13	Margin reefs backed by lagoonal facies. Mass-transported debris facies accumulate and interfinger with pelagic facies at the base of slope. Expansion of the reef margin into the lagoon during episodes of eustatic sea-level rise.	Rimmed platform	79	10
	2	264	6.5	0	n/a	13.5	1	5.5			18	11
	3	1475	19.5	1	12.2	After 4.64	2	17.5			76	12
	4	1475	15	1	12.3	After 4.64	4	11			68	13
	5	1461	18	6	16.4; 15.4; 10.8; 9.17; 8.88; 8.59	8.1	4	14	Margin reefs backed by lagoonal facies. Expansion of the reef margin into the lagoon during sea-level rises, in which lagoonal facies are drowned and buried locally by pelagic facies. Mass-transported debris facies interfinger with pelagic facies at the base of slope.		106	14
	6	3862	18	0		After 4.64	1.5	16.5	Margin reefs backed by lagoonal facies. As subsidence rates increase the reef facies, they expand into the platform interior, culminating in the demise of lagoonal facies at 9 Ma. A mass-transported debris facies accumulates on the margin slope and interfingers with pelagic facies. From 9 Ma onwards, carbonate production generated isolated pinnacle reefs.		121	15
	7	1475	18	1	12.5	After 4.64	2.5	15.5	Margin reefs backed by lagoonal facies. Mass-transport debris facies interfinger with pelagic facies at the base of slope. Expansion of the reef margin into the lagoon during episodes of eustatic sea-level rise.		73	16
	8	1475	16	1	12.5	After 4.64	2	14	Margin reefs backed by lagoonal facies. Mass-transport debris facies interfinger with pelagic facies at the base of slope. Expansion of the reef margin into the lagoon during episodes of eustatic sea-level rise. From 8.7 Ma onwards, the reef expands into the platform interior as lagoonal facies begin to cease production, with only the lagoonal factory producing carbonate strata.		70	17
	9	1000	11.5	1	12.5	8.7	0.5	11	Margin reefs backed by lagoonal facies. Mass-transport debris facies interfinger with pelagic facies at the base of slope. Expansion of the reef margin into the lagoon during episodes of eustatic sea-level rise. From 10.9 Ma onwards, sea-level rise causes the reef to expand into the platform interior as lagoonal facies cease production. During this period, pelagic facies onlap and bury the platform margin and its interior.		51	18

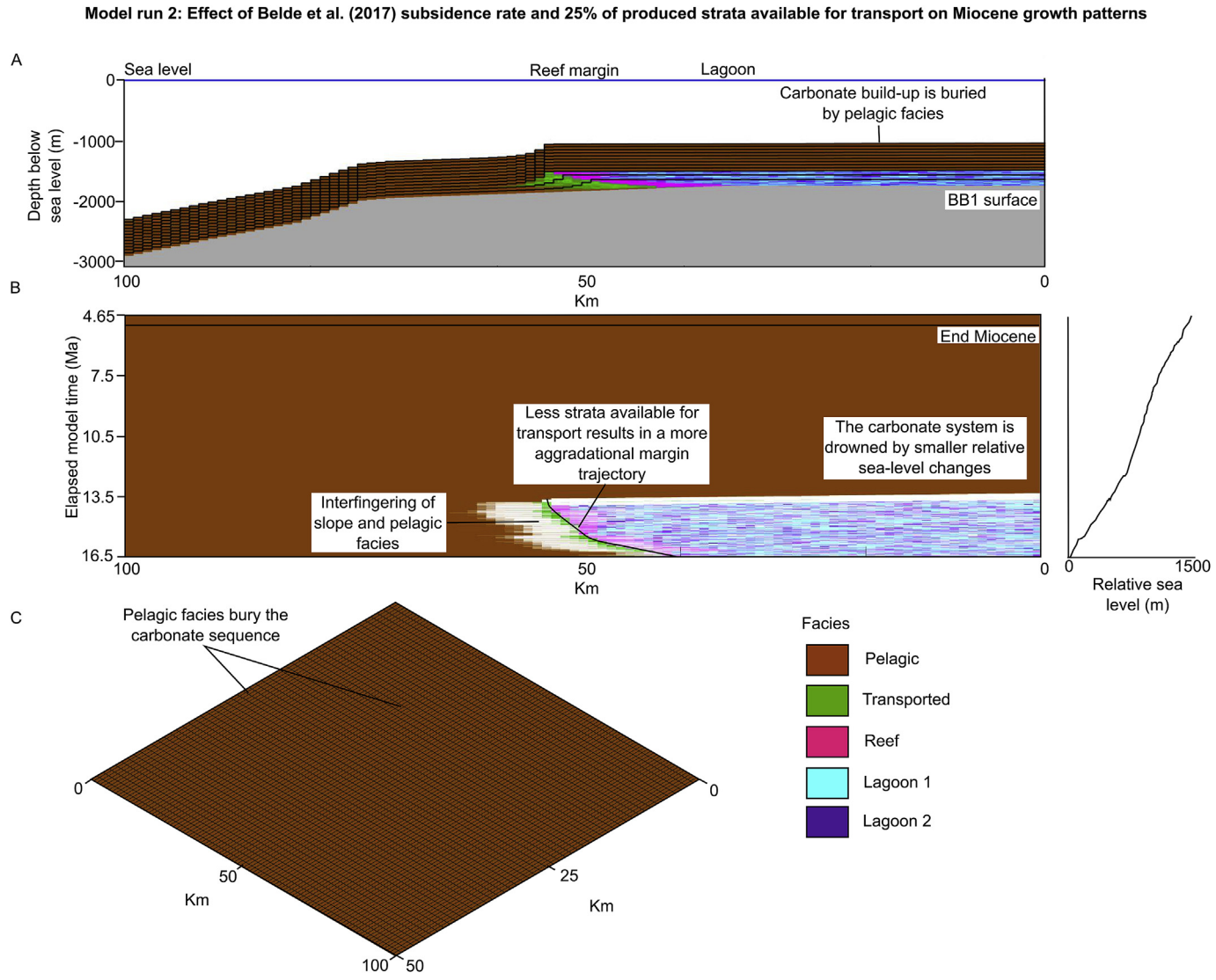

Fig. 11. CarboCAT Model Run 2 showing the effects of the Belde et al. (2017) variable subsidence profile, combined with the Miller et al. (2005) sea-level curve and 25% of produced facies available for transport (see Warrlich et al., 2008), on the growth patterns of the Miocene carbonate sequence. The model shows an initial progradational sequence drowned by 13.5 Ma. The carbonate sequence is characterised by a reef margin backed by a lagoon. A reduction in material available for transport made the carbonate sequence susceptible to smaller sea-level rises, when compared to Model Run 1.

importance of the parameters chosen (e.g. initial water depth vs. time-variable depth changes during the Miocene) to the final model results, b) the presence of karst horizons in the sequence boundaries imaged on seismic (Van Tuyl et al., 2018), c) the presence of subsurface phreatic cave systems (James and Choquette, 1990; Mylroie and Carew, 1990, 1995, Moore, 2001). Alternatively, the sequence boundaries imaged on seismic data may be associated with small patch-reefs, with intervening lagoons forming 'egg-box' topography as observed in the modern Great Barrier Reef. The step-out and step-down geometries associated with sequence boundaries on seismic data (Figs. 3 and 9) support the karst hypothesis and suggest that the subsidence rate proposed by Belde et al. (2017) is not valid for the study area. Eustatic sea-level amplitudes were also greater than the magnitude proposed by Miller et al. (2005) and could have attenuated subsidence to generate the exposure surfaces identified on seismic data.

Small-scale fluctuations in the position of the reef margin, relative to the lagoon, are observed in all model runs to suggest small-scale responses to eustatic sea level (Fig. 13). Such an interpretation agrees with the classification in Bosence (2005), indicating that eustatic sea level did not drive the large-scale morphology of the Browse Basin carbonate shelf; it was rather driven by small-scale variations in carbonate-facies distribution.

6.1.2. *Minimum average subsidence rates*

Using the eustatic sea-level curve in Miller et al. (2005), numerical modelling estimates a minimum average subsidence rate of 132 m/Ma to generate the 1475 m thick carbonate sequence interpreted in the northern Browse Basin (Figs. 9 and 13). This is a larger value than the averaged 125 m/Ma proposed by Belde et al. (2017) for the study area, but smaller than the modern day subsidence rates recorded to the north of the Browse Basin (290 m/Ma, Hengesh et al., 2010). These discrepant values of tectonic subsidence support the currently held hypothesis that subsidence rates along the North West Shelf increased with time as it migrated towards the Timor Trough (Rosleff-Soerensen et al., 2016; Belde et al., 2017). This is particularly documented in Model Run 6, which shows that progressive increases in subsidence can drive the change from a broad, large-scale rimmed platform to the isolated build-ups observed in the Browse Basin (Figs. 14 and 15). Thus, our results favour subduction-driven subsidence as the key control on accommodation space creation and large-scale carbonate growth patterns in the Browse Basin.

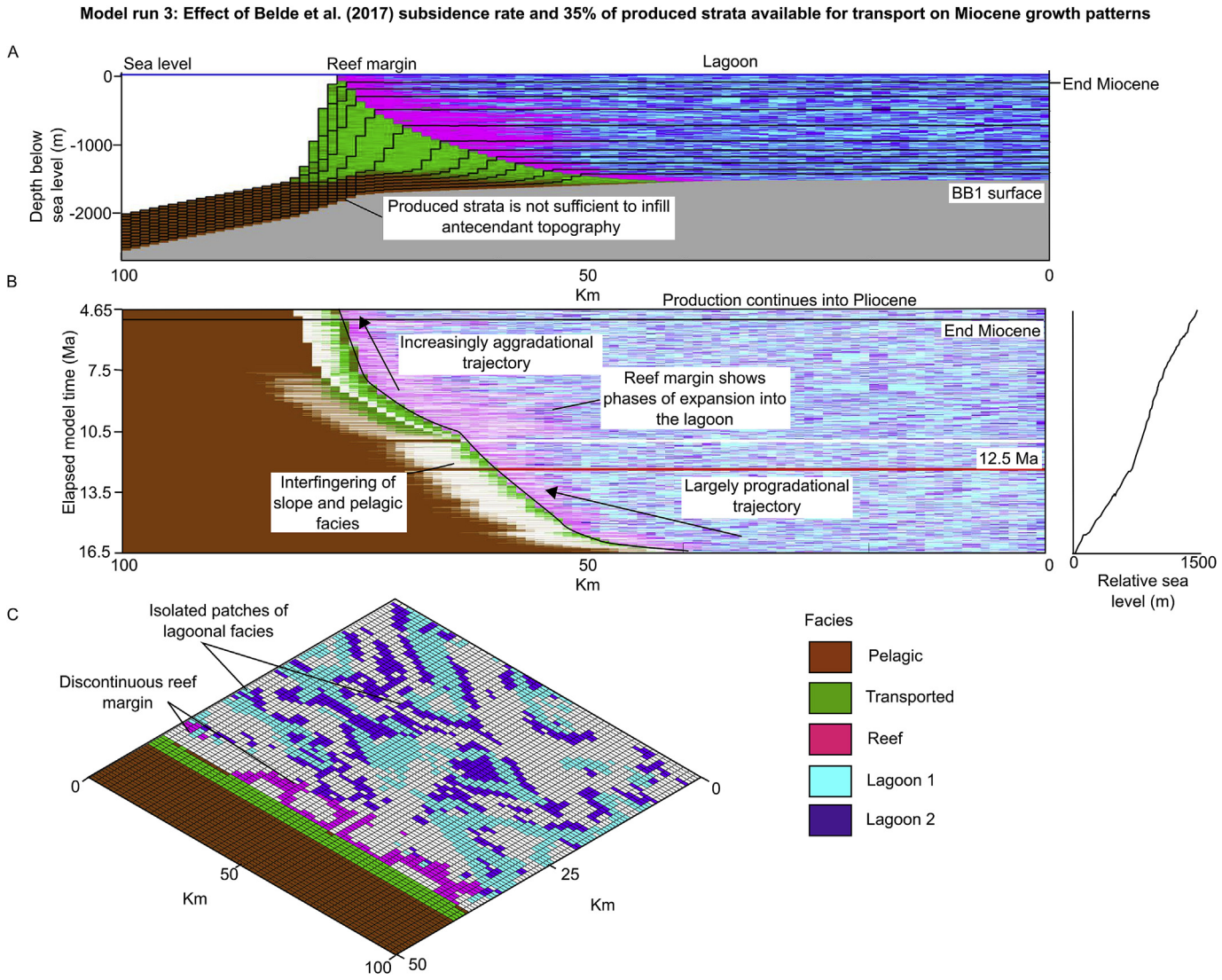

Fig. 12. CarboCAT Model Run 3 showing the effect the Belde et al. (2017) variable subsidence profile, combined with the Miller et al. (2005) sea-level curve and 35% of produced facies available for transport (see Warrlich et al., 2008), on the growth patterns of the Miocene carbonate sequence. The model shows an initial progradational sequence that transitions gradually towards an aggradational build-up. With less material available for transport, the pre-existing topography hinders the basinward progradation of the carbonate sequence. Sub-aerial exposure occurs at 12.5 Ma. The carbonate sequence is characterised by a reef margin backed by a lagoon. Carbonate production continues beyond the Miocene.

6.1.3. Regional depositional hiatus at ~12.5 Ma

An interesting outcome from the CarboCAT numerical modelling was that a sub-aerial exposure surface was generated in most Model Runs (except Model Runs 2 and 5) during the eustatic sea-level fall at 12.5 Ma and 12 Ma (Miller et al., 2005). This modelled sequence boundary falls just outside the ± 1 Ma error range for the interpreted age of the karst horizon capping Unit 2 (10–11 Ma), and is not synchronous to the sequence boundaries recorded at 15 Ma and 9 Ma in the southern Browse Basin (Rosleff-Soerensen et al., 2016). Instead, it is time-equivalent to sequence boundaries at 12 Ma and 13 Ma (± 1 Ma) recorded on the Queensland Plateau (QU 4 and QU 3), Marion Plateau (MSB3.3) and Great Bahama Bank (K and L) (Betzler et al., 2000; Eberli et al., 2010, 2002; John et al., 2011), suggesting that a major eustatic sea-level fall at around 12.5 Ma (Serravalian) led to emergence on both Northwest and Northeast Australia. The absence of a corresponding sequence boundary in the southern Browse Basin can be due to its associated features (e.g. karsts) being below seismic resolution and, therefore, rarely interpreted on seismic data from this same area. Alternatively, subsidence rates in the southern Browse Basin may have been faster than in the northern Browse Basin at this time, possibly in association with local faults attenuating the effects of the eustatic sea-level fall at 12.5–12 Ma.

6.1.4. Pulsed subsidence profile as explaining stratal geometry on seismic data

Model Run 5 tested a time-variable subsidence rate comprising alternating pulses of fast and slow subsidence (Figs. 4 and 14). Fig. 14 and Table 3 show a carbonate sequence that is first progradational but, in contrast to Model Runs 1 to 5 (Figs. 10–13), is forced to rapidly aggrade and split into isolated build-ups akin to the Browse Basin carbonate sequence (Fig. 5). The six (6) sub-aerial exposure events generated by Model Run 5 fall within 0.5 Ma of dated sequence boundaries (karst horizons) in the Browse Basin (Figs. 3, 9 and 14), as well as the inferred timing (Tortonian to Messinian) of karst horizons in the last stages of Miocene reef growth (Figs. 3 and 5). While the results of the numerical modelling do not provide an exact match to the interpreted seismic data in terms of build-up thickness (Table 3) our results suggest that, in order to replicate the Browse Basin carbonate sequence under the Miller et al. (2005) eustatic sea-level curve, a pulsed subsidence profile similar to that in Model Run 5 is required (Fig. 14).

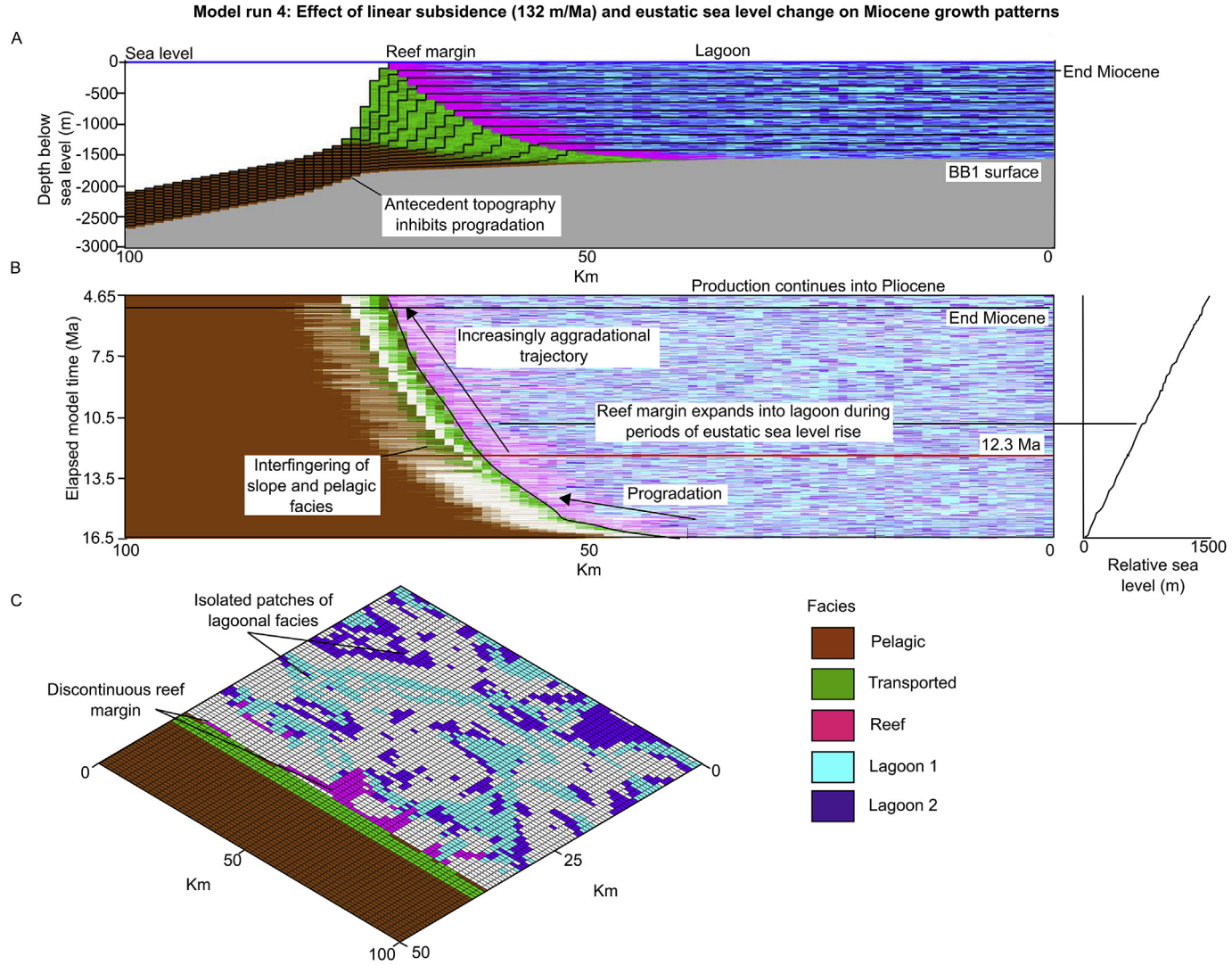

Fig. 13. CarboCAT Model Run 4 showing the effect of a 132 m/Ma linear subsidence rate, combined with the Miller et al. (2005) sea-level curve and 35% of produced facies available for transport (see Warrlich et al., 2008), on the growth patterns of the Miocene carbonate sequence. The model shows an initial progradational sequence that transitions to an aggradational build-up. With less material available for transport, the pre-existing topography hinders the basinward progradation of the carbonate sequence. Sub-aerial exposure occurs at 12.3 Ma. The carbonate sequence is characterised by a reef margin backed by a lagoon. Relative sea-level rise is not enough to drown the carbonate sequence by the end of the Miocene.

During episodic pulses of fast subsidence, the carbonate system was forced to rapidly aggrade or 'catch up' with relative sea-level rise (e.g. Unit 2, Van Tuyl et al., 2018), but was still able to enter a 'keep-up' phase during the intervening episodes of slow regional subsidence. This allowed eustatic sea-level falls to generate the interpreted exposure surfaces at 15 Ma (BB2), 11-10 Ma (BB3), and those in the Tortonian and Messinian (BB4 and BB5) (Figs. 3 and 5).

At this stage in the discussion is important to note three important aspects. Firstly, to generate comparable geometries to those observed on the seismic data requires a step-like subsidence profile not yet suggested for the North West Shelf, but observed on subduction margins such as Costa Rica's (Vannucchi et al., 2003). Secondly, subsidence rates in excess of 400 m/Ma were required on CarboCAT to generate comparable aggradational phases to those observed in the Poseidon-1 seismic volume; these are more than twice the rates proposed for the northern Browse Basin during the Miocene (125 m/Ma; Belde et al., 2017) and for the region to the north of this latter (290 m/Ma; Hengesh et al., 2010). While greater than the subsidence rates proposed in the literature, the values estimated in Models 1 to 9 fall short of the maximum subsidence rates of subduction margins, at around 1500 m/Ma (Galewsky et al., 1996). The absence of faults influencing carbonate evolution in the study area (see Van Tuyl et al., 2018) suggests that such subsidence rates are not due to fault movement, but rather varied significantly through the Miocene. Thirdly, while Model Run 5 replicated a basin evolution similar to that observed on seismic data (Fig. 14), it also suggests that the demise of the carbonate sequence occurred before the end of the Miocene. In the case of Model Run 5, this would be at around 8.1 Ma, falling between the proposed age of build-up demise between 10 and 5.33 Ma (Belde et al., 2017).

6.1.5. *The effect of antecedent topography on carbonate growth*

In all model runs, antecedent topography represented by the break in slope on the underlying Eocene-Oligocene carbonate ramp (BB1) imparted a control on margin geometry during the Miocene, notably inhibiting sediment progradation due to increasing water depths (Figs. 3 and 9). However, Model Runs 1 to 3 show that the percentage of produced carbonate facies available for transport is key to controlling the ability of the carbonate sequence to negate antecedent topography and promote sediment progradation beyond the break in slope (Figs. 10–12). The results of Model Runs 1 to 3 show that when the percentage of transportable material was set to 50%, sediment progradation exceeded that documented for the Browse Basin (Fig. 3 and

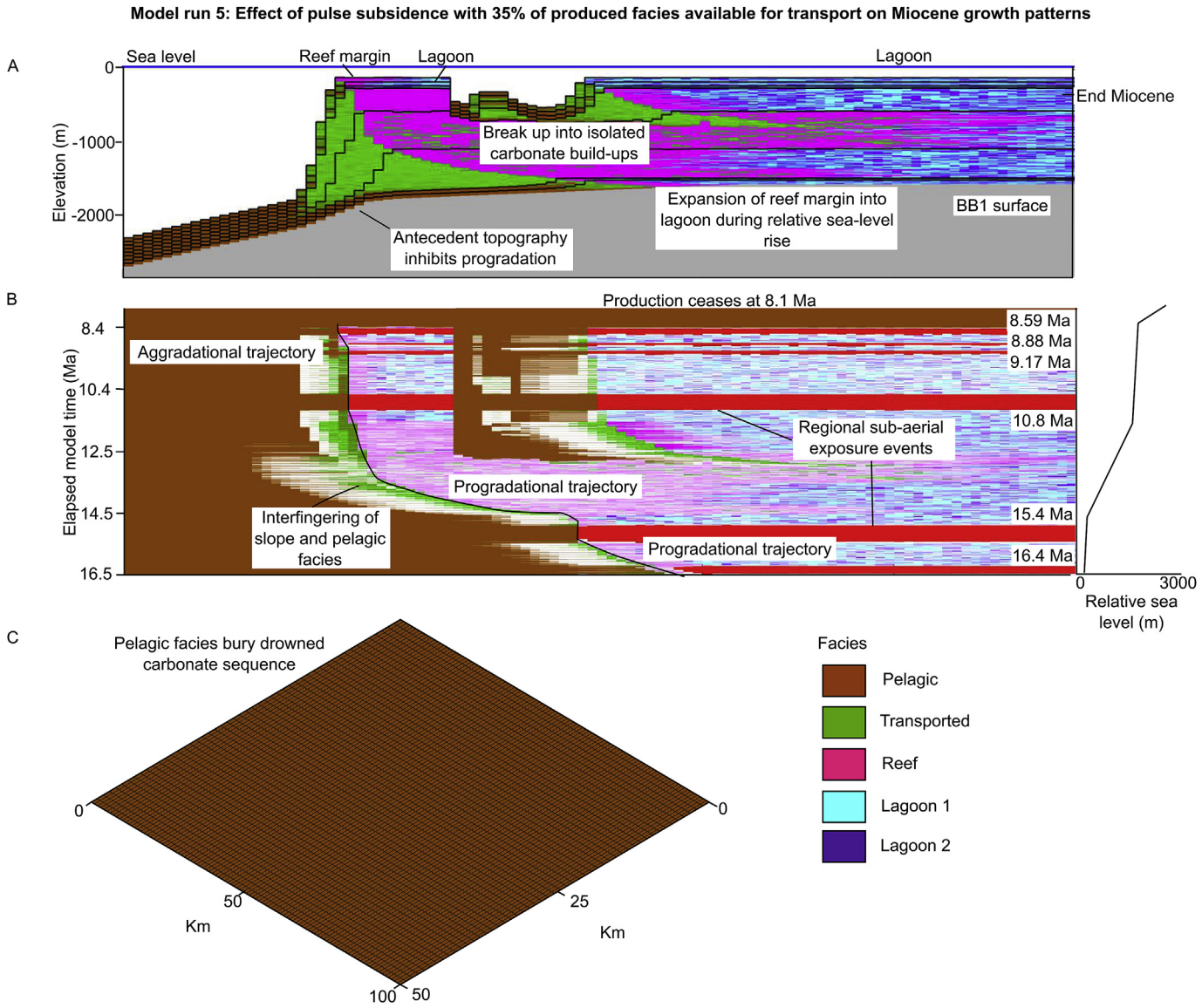

Fig. 14. CarboCAT Model Run 5 showing the effects of an experimental subsidence curve comprising pulses of fast and slow subsidence, combined with the Miller et al. (2005) sea-level curve and 35% of produced facies available for transport (see Warrlich et al., 2008), on the growth patterns of the Miocene carbonate sequence. The model shows an initial progradational sequence that transitions to an aggradational build-up. With less material available for transport, the pre-existing topography hinders the basinward progradation of the carbonate sequence. Six sequence boundaries are generated at 16.4 Ma, 15.4 Ma, 10.8 Ma, 9.17 Ma, 8.88 Ma and 8.59 Ma. The carbonate sequence is characterised by a reef margin backed by a lagoon. Relative sea-level rise facilitated by subsidence rates of 1400 m/Ma are sufficient to drown the carbonate sequence by 8.1 Ma.

Table 3). When the percentage of produced material available for transport was reduced to 35%, progradation geometries (and scales) became comparable to the seismic data (Table 3). However, when this same value was reduced to 25% the carbonate sequence became increasingly restricted and susceptible to smaller relative sea-level changes, resulting in its drowning. Thus, our results indicate that a relatively small percentage of produced carbonate material was available for transport in the study area when compared to the values proposed by Warrlich et al. (2008) for the Miocene. Furthermore, our results suggest that changes in transport rates through time, or the removal of carbonate sediment by currents (Adams and Hassler, 2010), influenced build-up growth and drowning at a local scale (Fig. 10).

6.2. *What was the primary control on the demise of carbonate build-ups offshore northwest Australia?*

The demise of Browse Basin's carbonate build-ups at the end of the Miocene has been speculatively attributed to rapid subsidence in conjunction with deteriorating environmental conditions (Rosleff-Soerensen et al., 2012, 2016; Howarth and Alves, 2016). Commonly, drowning carbonate sequences show aggradational growth patterns as production tries to keep up with sea-level rise. Seismic interpretation found no evidence for backstepping drowning geometries indicative of a rapid 'catch-up' phase prior to build-up demise. Instead, the flat-topped and karstified nature of the BB5 sequence boundary marking the end of Miocene carbonate build-up growth, suggests that carbonate build-ups were sub-aerially exposed prior to drowning and that no carbonate production was re-established thereafter in response to relative sea-level rise (Figs. 3 and 5). Hence, this latter interpretation reveals that: 1) under optimal environmental conditions, the rapid sea-level rise that followed the sub-aerial exposure of the build-ups was of sufficient amplitude, and over a short enough period of time, to drop the carbonate factories below the photic zone, thus shutting down carbonate production prior to the development of a subsequent

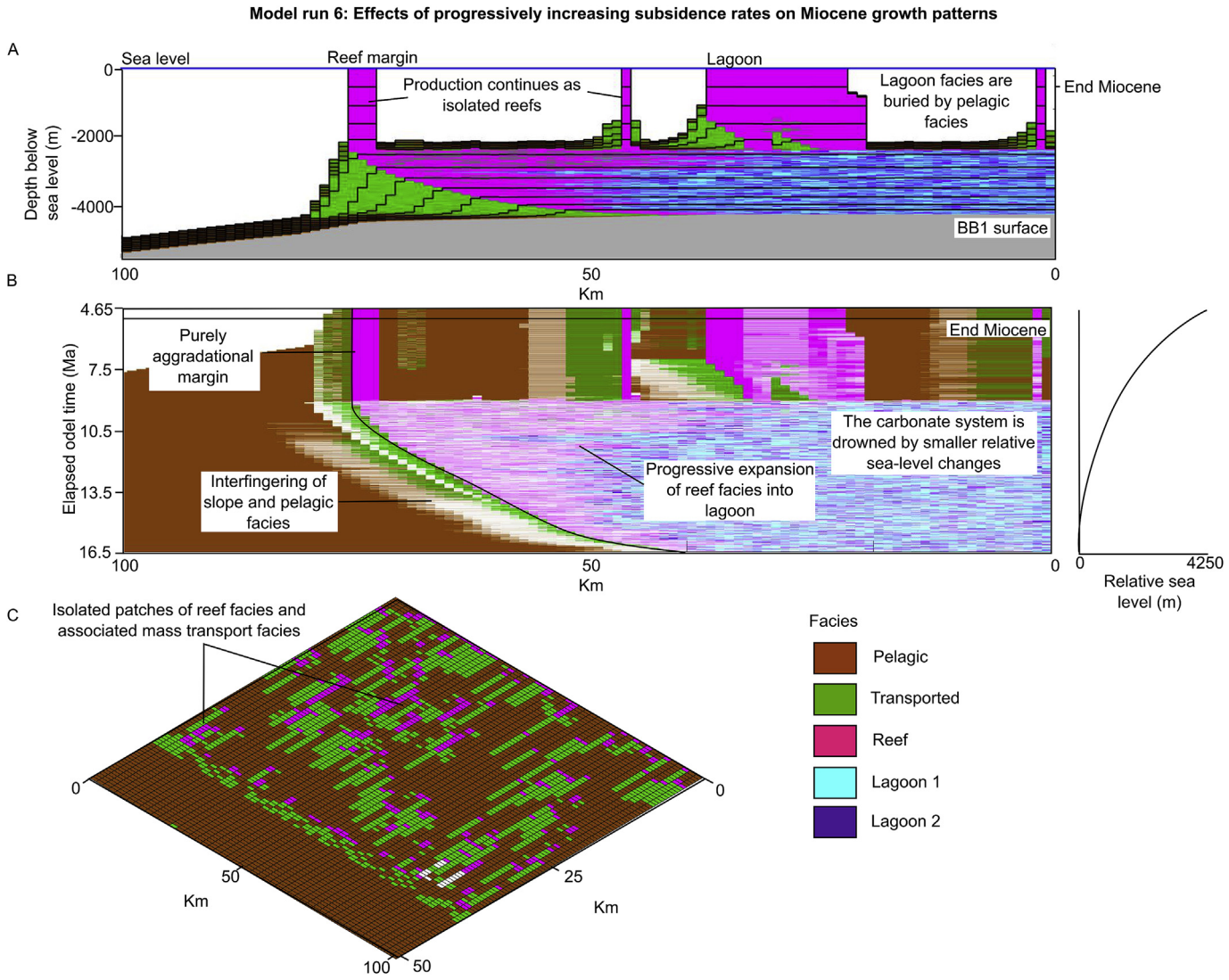

Fig. 15. CarboCAT Model Run 6 showing the effect of progressively increasing subsidence rates, applied to the Miller et al. (2005) sea-level curve and 35% of produced facies available for transport (see Warrlich et al., 2008), on Miocene growth patterns. The model shows that carbonate production is able to keep up with subsidence rates in excess of 620 m/Ma, more than twice the rate proposed for the Miocene northern Browse Basin and the modern North West Shelf of Australia. The carbonate sequence is characterised by a reef margin backed by a lagoon. As relative sea-level rises, reef facies expand into the interior and the lagoonal facies ceases production at 9 Ma. Relative sea-level change is insufficient to drown the carbonate sequence by the end of the Miocene.

Pliocene-Quaternary aggradational phase or, 2) environmental deterioration inhibited the carbonate factories in the northern Browse Basin and production could not keep-up with the subsequent Pliocene-Quaternary sea-level rise.

6.2.1. *Can the modelled subsidence rates justify build-up demise?*

Numerical modelling found that eustatic sea-level rise during the Late Miocene, when combined with subsidence rates above 132 m/Ma, were insufficient to drown the studied carbonate build-ups (Figs. 10–13). Instead, Model Runs 5 and 6 found that subsidence rates above 400 m/Ma caused significant geomorphological changes and drowned the lagoonal factories, while the reef factory was able to 'keep up' with subsidence rates in excess of 620 m/Ma. Complete drowning occurred when the subsidence rate exceeded 1100 m/Ma, creating the flat-topped topography observed on seismic data (Fig. 14). Such rates are above those proposed for the Browse Basin (Hengesh et al., 2010; Belde et al., 2017), but still within the range observed in subduction zones (Galewsky et al., 1996). As previously stated, the interpretation of the Poseidon 3-D seismic volume and regional 2-D profiles (Van Tuyl et al., 2018) found no evidence to support normal fault movement able to generate such subsidence rates, and thus influence growth patterns in the study area. Furthermore, the presence of the modern Seringapatam reef directly above the interpreted carbonate sequence on the basin margin (Fig. 1), indicates that parts of the study area have been in the photic zone during the Pliocene-Quaternary. This latter observation does not favour the notion that subsidence rates of ~1000 m/Ma characterised the final phase of carbonate growth in the Browse Basin and, therefore, they were not the primary cause of carbonate build-up demise.

6.2.2. *Current-driven sedimentation as a mechanism for build-up drowning*

Seismic interpretation identified numerous large-scale, mound-shaped packages, with low to moderate amplitude wavy reflections, close to carbonate build-ups, draping and burying them (Figs. 7 and 8). The geometry of these mounded seismic packages is comparable to current-driven sediment drifts in Faugères et al. (1999), Goktas et al. (2016) and Alves (2010), whereby sediments are carried by currents and deposited. Their appearance in the Miocene sequence correlates with Units 3 and 4 (Figs. 7–9). Lithological data from the Kronos-1 well do not provide the exact lithology of the sediment drifts. However, the

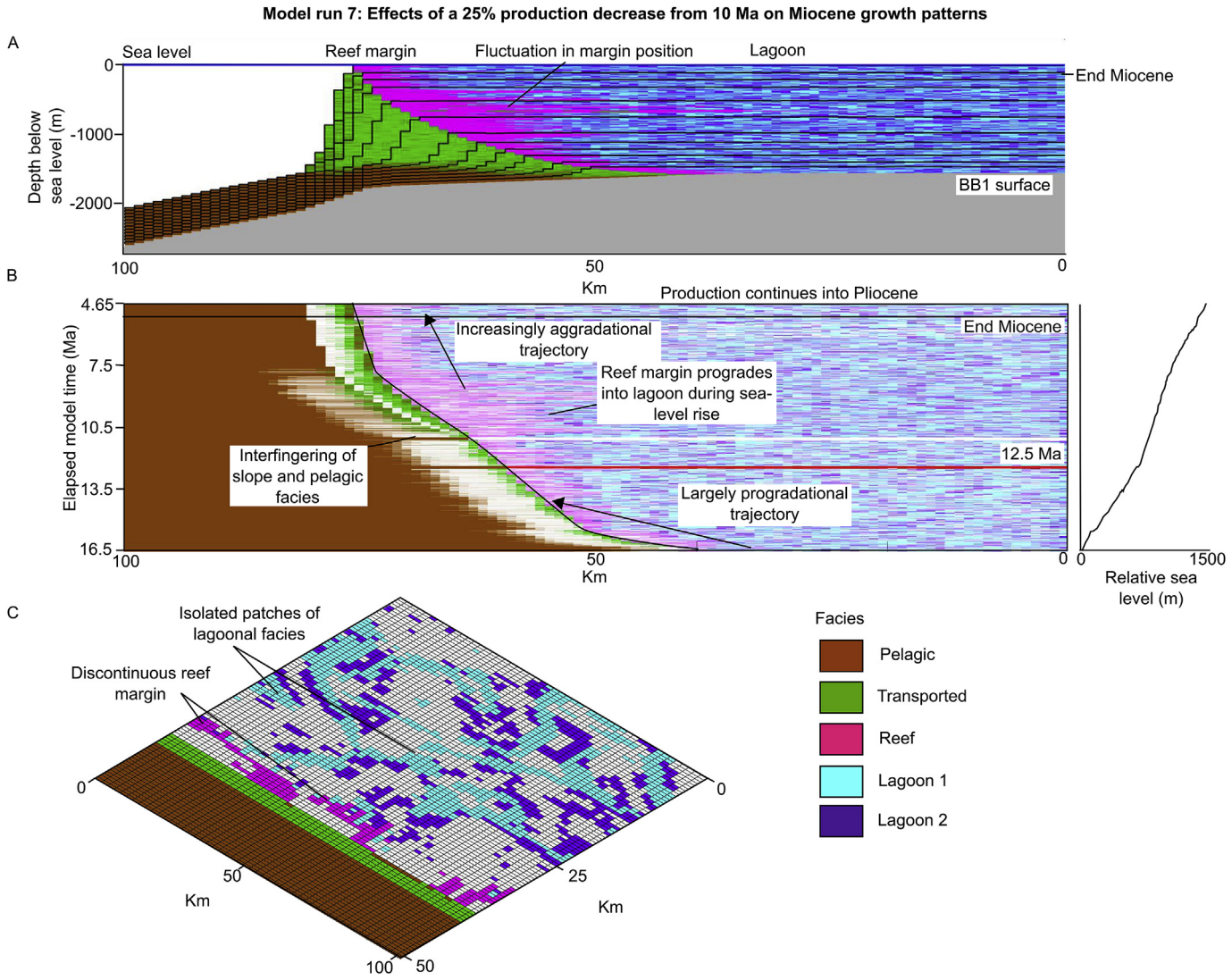

Fig. 16. CarboCAT Model Run 7 shows the effect of a 25% production decrease on carbonate growth patterns under the Belde et al. (2017) variable subsidence profile, combined with the Miller et al. (2005) sea-level curve and 35% of produced facies available for transport (see Warrlich et al., 2008). The model shows no visible effects on carbonate growth, with margin trajectory changing from progradational to aggradational to generate a sequence boundary at 12.5 Ma. A reef margin is backed by a lagoon and a debris deposit accumulated on the slope.

well reveals that sandy and silty sediment was fed to the carbonate system during the Late Miocene. Locally, the mound-shaped packages show onlapping relationships with carbonate build-ups and with each other, as well as truncations in internal reflections and negative V-shaped geometries suggestive of channels or moats (Figs. 6D and 8). This latter character indicates that the seabed topography imposed by the relatively older carbonate build-ups controlled the deposition of strata in Units 3 and 4, infilling topographic lows (Fig. 8). Hence, younger deposits were able to bury entire carbonate build-ups in a character comparable to the Nicholas Drift overlying the Cretaceous carbonate platform of the Great Bahama Bank (Jo, 2013).

Modelling the effect of current-driven deposits on carbonate production found that, when production rates decrease over 50%, carbonate factories become increasingly susceptible to eustatic sea-level changes (Davies et al., 1991; Isern et al., 2004; Betzler et al., 2009). Pronounced changes in build-up geomorphology, and the drowning sequence per se, were generated in Model Runs 8 and 9 (Figs. 16–18), similar to what is observed in Units 3 and 4. Model Run 8 showed a comparable fragmentation of the larger build-up into isolated build-ups, with localised drowning between Units 2 and 3 (Fig. 17). However, complete drowning was not achieved in Model 8 at the end of the Miocene (Fig. 17).

Model Run 9 considered a 75% decline in carbonate production, resulting in near-immediate drowning and flat-topped morphologies comparable to the build-ups observed in Unit 4 (Figs. 3 and 18). While Model Runs 8 and 9 did not replicate the exact geometries and equivalent sequence boundaries to the northern Browse Basin's (Figs. 9, 17 and 18), their outputs show that the influx of current-driven sediment facilitated the drowning of the carbonate sequence without the need for subsidence rates in the scale of 1100 m/Ma and above (Model Runs 5 and 6). Differences in build-up geometries between Model Runs 8 and 9, when compared to seismic data (Fig. 3), can thus be explained by the progressive importance of current-driven sedimentation during the Late Miocene, leading to a transition from the scenario suggested by Model Run 8 during Unit 2 and 3, to Model Run 9 during Unit 4 (Figs. 16 and 18).

A relationship between sediment drifts and carbonate demise is documented by Betzler et al. (2013) in the Maldives. The influx of current-driven sediment brings additional nutrients onto carbonate platforms and promotes the development of larger benthic organisms, thus increasing competition for space on the seabed (Mutti and Hallock, 2003), and increasing bio-erosion rates capable of suppressing net

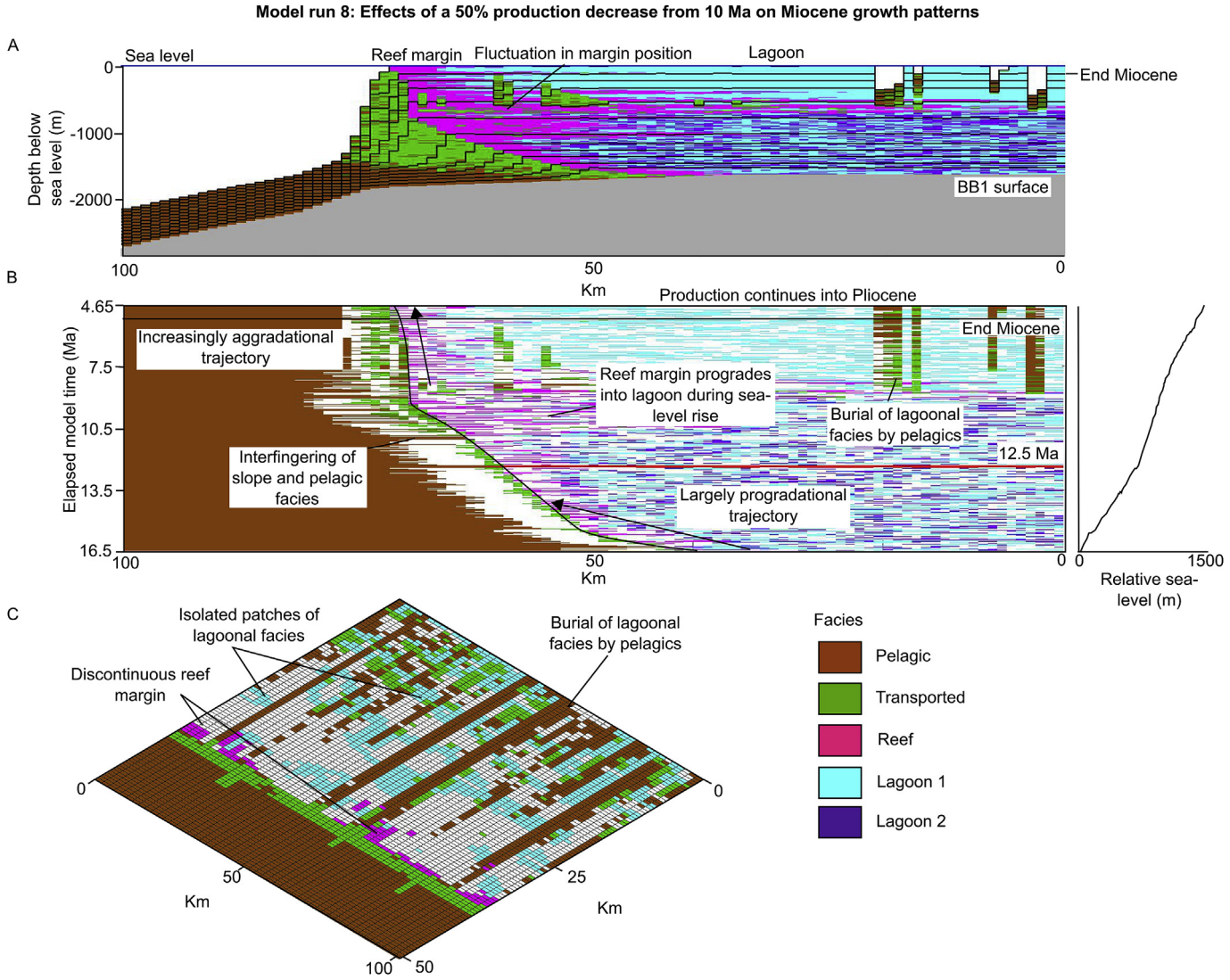

Fig. 17. CarboCAT Model Run 8 shows the effect of a 50% production decrease on carbonate growth patterns under the Belde et al. (2017) variable subsidence profile, combined with the Miller et al. (2005) sea-level curve and 35% of produced facies available for transport (see Warrlich et al., 2008). The model shows that carbonate build-ups become susceptible to sea-level rise as production rates decrease; the 8.7 Ma eustatic sea-level rise causing significant geomorphological changes in the carbonate sequence. The reef margin facies expands into the platform interior, where lagoonal factories shut-down and are drowned and buried by pelagic facies. Pinnacle-reef geometries aggrade rapidly in response to fast relative sea-level rise. By the end of the model run, large areas of the carbonate build-up are drowned, but a scattered reef margin persists.

framework production (Mutti and Hallock, 2003). It also stops photosynthetic coral builders from producing reef frameworks (Betzler, 1997; Carannante et al., 1988; Hallock, 1988; Mutti and Hallock, 2003). Matching processes able to suppress carbonate production in the northern Browse Basin were sub-aerial exposure and karstification of sequence boundary BB5 (Figs. 3 and 6).

6.2.3. *Global-scale phenomena promoting build-up demise*

The outputs of Model Runs 8 and 9 show that declining carbonate production generates a comparable drowning sequence to that interpreted on the seismic data (Figs. 9, 17 and 18). An alternative explanation for suppressed production is global cooling associated with the end of the Mid-Miocene Climate Optimum (Isern et al., 1996), when the global climate transitioned to the modern Icehouse conditions (Zachos et al., 2001; Foster et al., 2012). Southern hemisphere glaciation began at this time (Shackleton and Kennett, 1975; Kastens, 1992), and the resulting expansion of the southern hemisphere ice sheet (Ryan et al., 1974; Kastens, 1992) decreased ocean temperatures from 14.5 Ma onwards (Böhm, 2003). In addition, the proposed restriction of the Indonesian seaway and the resulting diversion of the warm Indonesian Throughflow through the Timor Passage away from the Browse Basin (O'Brien et al., 2002), would have reduced the influx of warm waters into the study area at the end of the Miocene, further decreasing sea temperatures below the optimum value of 22 °C (Mutti and Hallock, 2003). This phenomenon generated a mechanism to drown carbonate build-ups through environmental deterioration.

Notwithstanding the latter postulates, the presence of the modern day Seringapatam reef in the study area indicates that ocean temperatures remained sufficiently warm to support carbonate production, agreeing with Belde et al. (2017), who proposed that the expansion of the tropical warm pool during the Pliocene maintained sea-surface temperatures of 23–27 °C in the Browse Basin (see also Karas et al., 2011). Consequently, the evidence presented in this paper does not favour demise through cooling, but rather through the influx of current-driven sediment (Fig. 19).

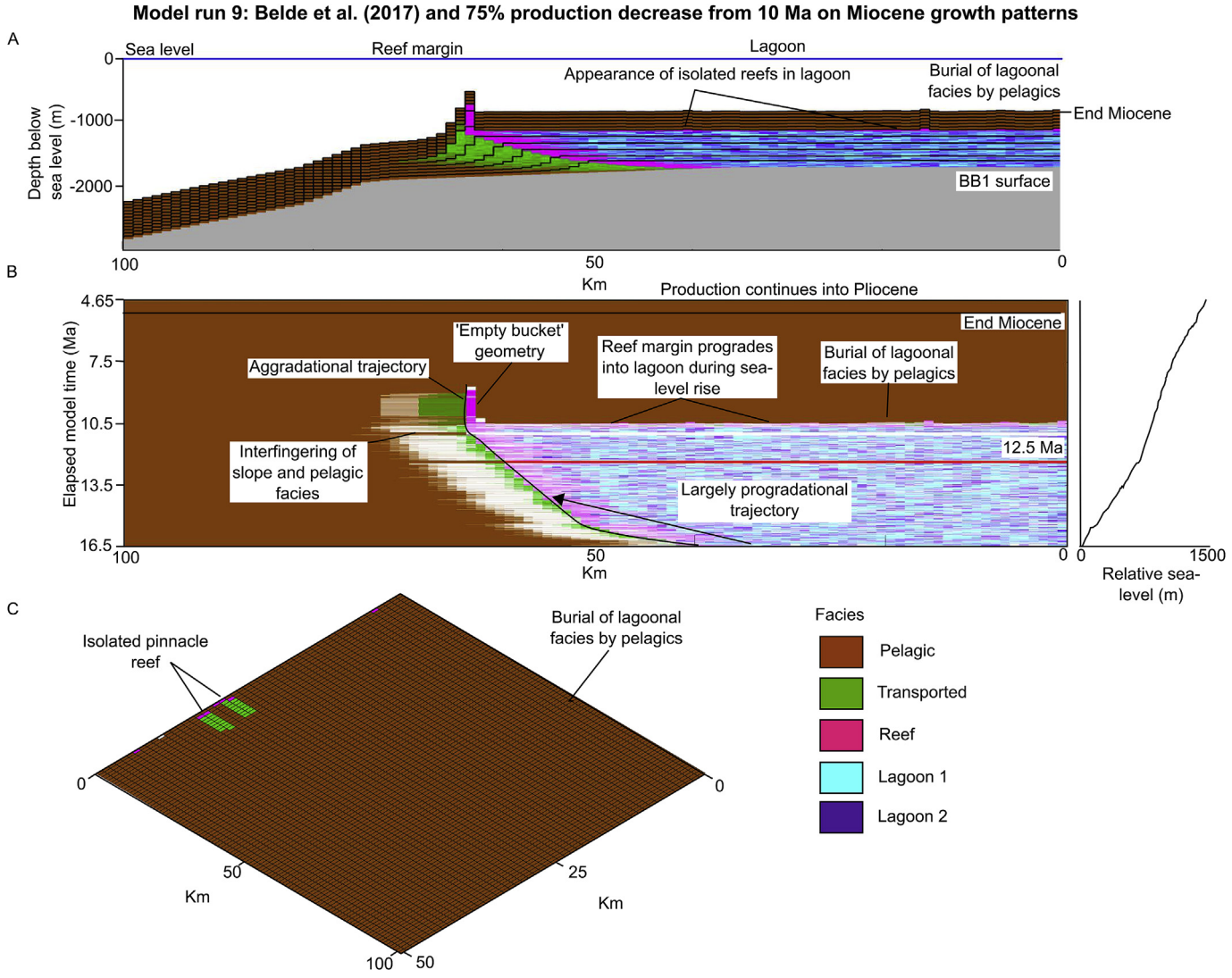

Fig. 18. CarboCAT Model Run 9 shows the effect of a 75% production decrease on carbonate growth patterns under the Belde et al. (2017) variable subsidence profile, combined with the Miller et al. (2005) sea-level curve and 35% of produced facies available for transport (see Warrlich et al., 2008). The model shows that a 75% production decline results in the rapid demise of the carbonate build-up as carbonate factories become highly susceptible to small eustatic sea-level rises. The results also show that lagoonal production is shut-down almost immediately at 10.6 Ma, with subtle patch-reefs appearing in the platform interior until 10.51 Ma. Reef production continues on the margin as an isolated pinnacle that is drowned and buried by pelagic facies at ~8.7 Ma.

6.3. Model constraints

The numerical modelling in this work carbonate system proved its importance to understand the effects of time-variable processes on carbonate evolution at a regional scale. The results of the CarboCAT numerical modelling generated growth patterns and assigned carbonate facies that are comparable to the interpreted seismic volume, reflecting the complexity and heterogeneity that are characteristic of carbonate systems.

Comparing the scale relationships between the computed numerical models (Figs. 10–18), and seismic interpretation (Figs. 3 and 6), shows that models are valuable in revealing the evolution of basin-scale carbonate systems. Our results replicate all the key features observed readily in the Poseidon-1 seismic volume (progradation, aggradation, sub-aerial exposure) required to derive the relative significance of different time-dependent processes. Naturally, the 500 m by 500 m cell size used in the modelling induces over-simplification in the outputs by some degree, as it averages data and leads to the omission of finer-scale features such as lowstand systems tracts associated with sub-aerial exposure (Figs. 10–18), which are often (but not always) observed on seismic data (Figs. 3 and 6A). Another caveat of using 500 m by 500 m cell sizes concerns the over-representation of depositional facies, such as those of the reef margin spanning over a distance exceeding 6 km in Model Run 5 (Fig. 14). Nevertheless, within the remit of this work, the CarboCAT models allowed us to investigate the effects of different time-variable processes and derive their relative significance.

The effects of compaction also need to be considered in the modelling of carbonate platforms. As carbonates are buried, mechanical and chemical compaction drive porosity reduction due to: a) increasing vertical loads applied on the sediment by overburden strata, b) thermodynamic processes, and c) fluid-rock interactions (Croizé, 2010). Buried under 434 m of sediment (Kronos-1 well, ConocoPhillips, 2011b), one should expect some degree of compaction affecting the interpreted carbonate sequence. However, with no well or core data to constrain the degree of compaction experienced by different strata in the Browse Basin, differential compaction was not considered in the model runs and, therefore, they should be treated as computing pre-compaction thicknesses.

It is important to also consider the reliability of the input parameters chosen for the regional models (Tables 1 and 2). In this work,

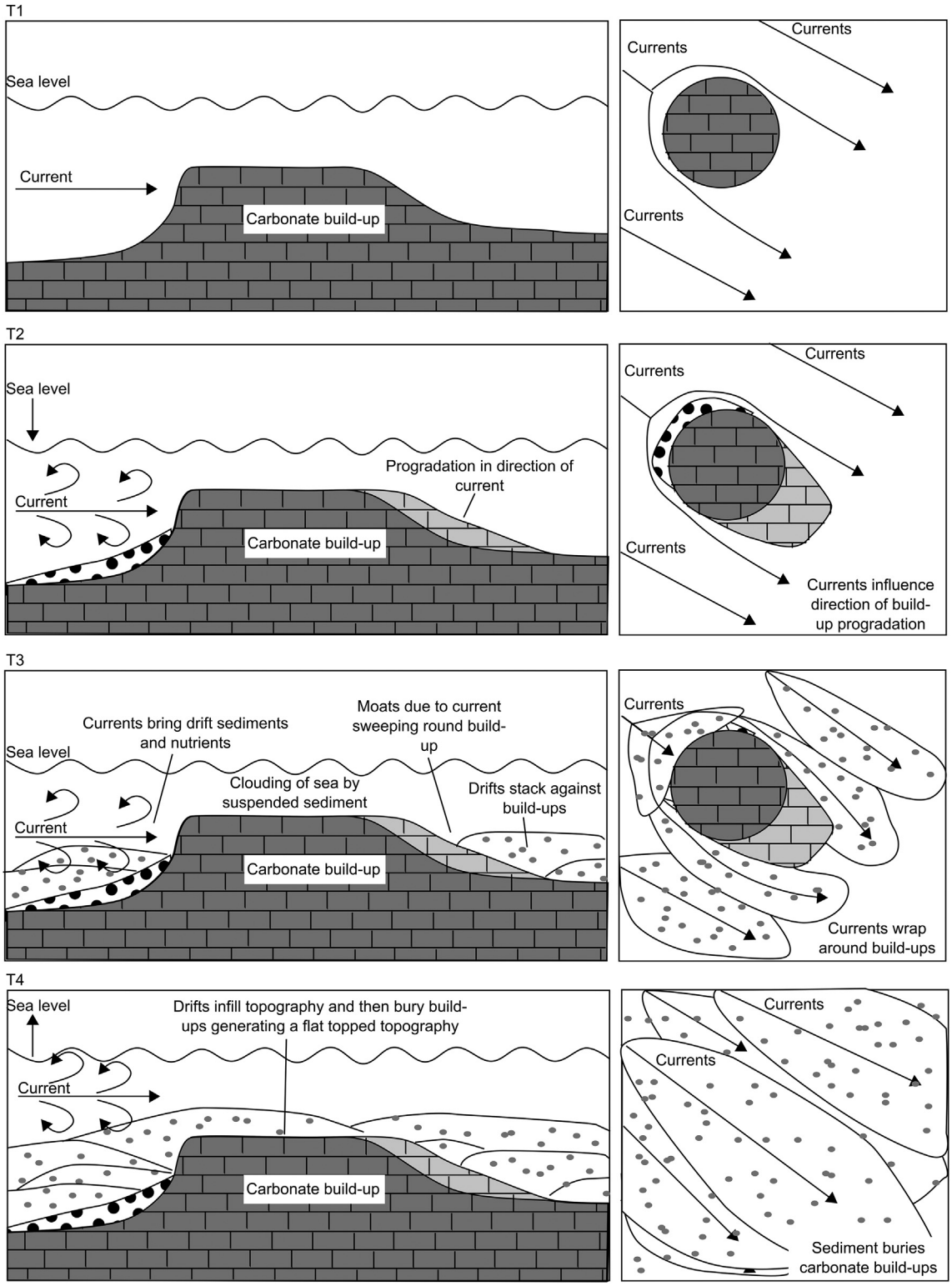

Fig. 19. Cartoon showing a summary of the demise of carbonate build-ups due to the onset of a current-dominated system, bringing sediment and nutrients into the Browse Basin. Initially, the carbonate build-ups grow in optimum conditions. The onset of T2 sees currents increase in strength, forcing progradation. Thereafter, currents bring current-driven sediment that initially stack against build-ups. Suspended sediment and excess nutrients are enough to suppress production by increasing competition and decreasing the light transmissivity of the water column during T3. Finally, current-driven sediment fills the topography and subsequently envelop the build-ups.

input values such as production profiles are taken from analogues (e.g. Warrlich et al., 2008), the initial bathymetry is derived from detailed seismic interpretation (e.g. BB1), and eustatic sea-level curves are based on the published literature (e.g. Miller et al., 2005), making these outputs robust with respect to the current understanding. Initial water depth, while difficult to determine accurately, is constrained within a range based on our seismic interpretation. In contrast, spatial competition between carbonate factories is still difficult to constrain based on the current literature. Based on this same literature, and the new seismic interpretation in this work (e.g. Kenter, 1990; Warrlich et al., 2002, 2008; Belde et al., 2017; Van Tuyl et al., 2018) the CarboCAT models are considered robust when applied to the study area. Naturally, they can only be improved as more data becomes available and models are revisited.

7. Conclusions

Based on the interpretation of high-quality 3-D seismic data from the northern Browse Basin, and CarboCAT numerical modelling, this work reached the following conclusions:

1) Published and new seismic interpretations have been tested by forward CarboCAT modelling, suggesting that stratal architectures on 3-D seismic data cannot be generated by the eustatic sea-level fluctuations and subsidence rates currently assumed for the Browse Basin.
2) A subsidence profile comprising pulses of rapid and slow subsidence is required to enhance relative sea-level changes so that sequence boundaries are generated in a pattern similar to that observed on seismic data.
3) A subsidence rate of ~400 m/Ma is required to generate aggradational geometries similar to the 3-D seismic data. This is a value significantly higher than that currently proposed in the literature.
4) Environmental deterioration in the form of current-driven sediment was key to the demise of the Miocene carbonate sequence in the Browse Basin. Sediment drifts buried some carbonate build-ups, while suspended drift sediment reduced the transmissivity of sunlight in the water column, inhibiting production and making it susceptible to subsequent eustatic sea-level rises.
5) Numerical modelling proved an effective tool to derive the relative importance of time-variable processes on Miocene reef growth. However, it is important to consider the effects of up- and downscaling the model results. Notably, the size of geobodies, such as the reef margin, are likely over-estimated when modelling at the cell sizes of 500 m by 500 m adopted in this work. Similarly, the absence of lowstand systems tracts during sub-aerial exposure may be a function of depth changes across two distinct cells.

Acknowledgements

We thank the support of the NERC Centre of Doctoral Training in Oil and Gas (NERC Oil and Gas CDT Grant NE/M00578X/1), which was co-sponsored by Cardiff University. Schlumberger provided (Petrel) academic licenses to Cardiff University. This work used data from Geosciences Australia, whom we duly acknowledge. We thank C. Elders and C. Hollis for their constructive reviews.

Appendix A. Supplementary data

Supplementary data to this article can be found online at https://doi.org/10.1016/j.marpetgeo.2019.03.006.

References

Eberli, G.P., Anselmetti, F.S., Kroon, D., Sato, T., Wright, J.D., 2002. The chronostratigraphic significance of seismic reflections along the Bahamas Transect. Mar. Geol. 185, 1–17.
Ryan, W.B.F., Cita, M.B., Rawson, M.D., Burckle, L.H., Saito, T., 1974. A paleomagnetic assignment of Neogene stage boundaraies and the development of isochronous datum planes between the Mediterranean, the Pacific and Indian Oceans in order to investigate the response of the World Ocean to the Mediterranean "Salinity Crisis". Riv. Ital. Paleontol. Stratigr. 80, 631–688.
Saqab, M.M., Bourget, J., 2016. Seismic geomorphology and evolution of early-mid Miocene isolated carbonate build-ups in the Timor Sea, North West Shelf of Australia. Mar. Geol. 379, 224–245.
Struckmeyer, H.I.M., Blevin, J.E., Sayers, J., Totterdell, J.M., Baxter, K., Cathro, D.L., 1998. Structural evolution of the Browse basin, North West Shelf: new concepts from deep-seismic data. In: Purcell, P.G., Purcell, R.R. (Eds.), 1998, the Sedimentary Basins of Western Australia 2: Proceedings of Petroleum Exploration Society of Australia Symposium, Perth, WA, pp. 345–367.
Adams, E.W., Hassler, C.A., 2010. The intrinsic effect of shape on retrogradation motif and timing of drowning of carbonate patch reef systems (Lower Frasnian, Bugle Gap, Canning Basin, Western Australia). Sedimentology 57, 956–984. https://doi.org/10.1111/j.1365-3091.2009.01127.x.
Alves, T.M., 2010. A 3-D morphometric analysis of erosional features in a contourite drift from offshore SE Brazil. Geophys. J. Int. 183 (3), 1151–1164.
Antonatos, G., 2018. Effect of Carbonate Platform Controls on Large Scale Platform Heterogeneity and Seismically Imaged Geometries. PhD thesis. Royal Holloway, University of London.
Apthorpe, M., 1988. Cainozoic depositional history of the North West shelf. In: Purcell, P.G., Purcell, R.R. (Eds.), Proceedings of Petroleum Exploration Society of Western Australia Symposium, Perth. The North West Shelf, Australia, pp. 55–84.
Belde, J., Back, S., Bourget, J., Reuning, L., 2017. Oligocene and Miocene carbonate platform development in the Browse Basin, Australian northwest shelf. J. Sediment. Res. 87, 795–816.
Betzler, C., 1997. Ecological controls of geometries of carbonate platforms: Miocene/Pliocene shallow-water Microfaunas and carbonate biofacies from the Queensland Plateau (NE Australia). Facies 37, 147–166.
Betzler, C., Kroon, D., Reijmer, J.J.G., 2000. Synchroneity of major late Neogene sea-level fluctuations and paleoceanographically controlled changes as recorded by two carbonate platforms. Paleoceanography 15, 722–730.
Betzler, C., Hübscher, C., Lindhorst, S., Reijmer, J.J.G., Römer, M., Droxler, A.W., Fürstenau, J., Ludmann, T., 2009. Monsoon-induced partial carbonate platform drowning (Maldives, Indian Ocean). Geology 37, 867–870. https://doi.org/10.1130/G25702A.1.
Betzler, C., Fürstenau, J., Lüdmann, T., Hübscher, C., Lindhorst, S., Paul, A., Reijmer, J.J.G., Droxler, A.W., 2013. Sea-level and ocean-current control on carbonate- platform growth, Maldives, Indian Ocean. Basin Res. 25, 172–196.
Betzler, C., Lindhorst, S., Lüdmann, T., Weiss, B., Wunsch, M., Braga, J.C., 2015. The leaking bucket of a Maldives atoll: implications for the understanding of carbonate platform drowning. Mar. Geol. 366, 16–33.
Betzler, C., Hübscher, C., Lindhorst, S., Lüdmann, T., Reijmer, J.J., Braga, J.C., 2016. Lowstand wedges in carbonate platform slopes (Quaternary, Maldives, Indian Ocean). The Depositional Record 2, 196–207.
Blevin, J.E., Struckmeyer, H.I.M., Cathro, D.L., Totterdell, J.M., Boreham, C., Romine, K.K., Loutit, T.S., Sayers, J., 1998. Tectonostratigraphic framework and petroleum systems of the Browse Basin, North West Shelf. In: Purcell, P.G., Purcell, R.R. (Eds.), The Sedimentary Basins of Western Australia 2: Proceedings of the Petroleum Exploration Society of Australia Symposium, Perth, pp. 369–420.
Böhm, M., 2003. The Miocene climatic optimum: evidence from ectothermic vertebrates of Central Europe. Palaeogeogr. Palaeoclimatol. Palaeoecol. 195 (3–4), 389–401.
Bosence, D., 2005. A genetic classification of carbonate platforms based on their basinal and tectonic settings in the Cenozoic. Sediment. Geol. 175, 49–72.
Bosscher, H., Schlager, W., 1992. Computer simulation of reef growth. Sedimentology 39, 503–512.
Brachert, T.C., Reuter, M., Kroeger, K.F., Lough, J.M., 2006. Coral growth bands: a new and easy to use paleothermometer in paleoenvironment analysis and paleoceanography (late Miocene, Greece). Paleoceanography 21, PA4217.
Burgess, P.M., 2013. CarboCAT: a cellular automata model of heterogeneous carbonate strata. Comput. Geosci. 53, 129–140.
CALENERGY Resources (Australia) LTD, 2013. Browse Basin Offshore Drilling Campaign, WA-424-P. Environment Plan Summary. pp. 1–27.
Carannante, G., Esteban, M., Milliman, J.D., Simone, L., 1988. Carbonate lithofacies as paleolatitude indicators: problems and limitations. Sediment. Geol. 60, 333–346.
ConocoPhillips, 2010. Poseidon-1 Well Completion Report, vol. 1. Basic Data, pp. 1–1133.
ConocoPhillips, 2011a. Poseidon-2 Well Completion Report, vol. 1. Basin Data, pp. 1–1466.
ConocoPhillips, 2011b. Kronos-1 Well Completion Report, vol. 2. Interpretive Data, pp. 1–954.
ConocoPhillips, 2012. WA-315-P and WA398-P Browse Basin Western Australia 2009 Poseidon 3D Marine Surface Seismic Survey: Interpretation Report. pp. 1–43.
Croizé, D., 2010. Mechanical and Chemical Compaction of Carbonates – an Experimental Study. Ph.D. Thesis. University of Oslo, pp. 1–176.
Davies, P.J., McKenzie, J.A., Palmer-Julson, A., et al., 1991. Proceedings of the Ocean Drilling Program, Initial Reports. Ocean Drilling Program, vol. 133. Texas A&M University, College Station, Texas, pp. 810.
Eberli, G.P., Anselmetti, F.S., Isern, A.R., Delius, H., 2010. Timing of changes in sea-level and currents along Miocene platforms on the Marion Plateau, Australia. In: In: Morgan, W.A., George, A.D., Harris, P.M., Kupecz, J.A., Sarg, J.F. (Eds.), Cenozoic Carbonate Systems of Australasia, vol. 95. SEPM Special Publication, pp. 219–242.
Faugères, J.-C., Stow, D.A.V., Imbert, P., Vianna, A., 1999. Seismic features diagnostic of contourite drifts. Mar. Geol. 162 (1), 1–38.

Foster, G.L., Lear, C.H., Rae, J.W.B., 2012. The evolution of pCO^2, ice volume and climate during the middle Miocene. Earth Planet. Sci. Lett. 341–344, 243–254.
Galewsky, J., Silver, E.A., Gallup, C.D., Edwards, R.L., Potts, D.C., 1996. Foredeep tectonics and carbonate platform dynamics in the Huon Gulf, Papua New Guinea. Geology 24 (9), 819–822.
Gallagher, S.J., Wallace, M.W., Hoiles, P.W., Southwood, J.M., 2014. Seismic and stratigraphic evidence for reef expansion and onset of aridity on the Northwest Shelf of Australia during the Pleistocene. Mar. Petrol. Geol. 57, 470–481.
Goktas, P., Austin, J.A., Fulthorpe, C.S., Gallagher, S.J., 2016. Morphologies and depositional/erosional controls on evolution of Pliocene–Pleistocene carbonate platforms. Northern Carnarvon Basin, Northwest Shelf of Australia: Cont. Shelf Res. 124, 63–82.
Hallock, P., 1988. Diversification in algal symbiont-bearing foraminifera: a response to oligotrophy? Vol. Spec. 2. Rev. Paleobiology 789–797 (Benthos '86).
Hallock, 2006. Global change and modern coral reefs: new opportunities to understand shallow-water carbonate depositional processes. Sedimentology 175, 19–33.
Hallock, P., Schlager, W., 1986. Nutrient excess and the demise of coral reefs and carbonate platforms. Palaios 1, 289–298.
Haq, B.U., Hardenbol, J., Vail, P.R., 1987. Chronology of fluctuating sea levels since the Triassic (250 million years ago to present). Science 235 (1) 156–1,167.
Harrowfield, M., Keep, M., 2005. Tectonic modification of the Australian North-West Shelf: episodic rejuvenation of long-lived basin divisions. Basin Res. 17 (2), 225–239.
Haston, R.B., Farrelly, J.J., 1993. Regional significance of the aequebus 1 well, Browse basin, North West Shelf, Australia. APEA J. 33 (1), 28–38.
Hengesh, J.V., Wywroll, K.-H., Whitney, B.B., 2010. Neotectonic deformation of northwestern Australia: implications for Oil and gas developments. In: International Symposium on Frontiers in Offshore Geotechnics, Conference Proceedings.
Howarth, V., Alves, T.M., 2016. Fluid flow through carbonate platforms as evidence for deep-seated reservoirs in North West Australia. Mar. Geol. 380 (1), 17–43.
Hull, J.N.F., Griffiths, C.M., 2002. Sequence Stratigraphic Evolution of the Albian to Recent Section of the Dampier Sub-basin. North West Shelf Australia, pp. 617–639.
Isern, A.R., McKenzie, J.A., Feary, D.A., 1996. The role of sea-surface temperature as a control on carbonate platform development in the western Coral Sea. Palaeogeogr. Palaeoclimatol. Palaeoecol. 124, 247–272.
Isern, A.R., Anselmetti, F.S., Blum, P., 2004. A Neogene carbonate platform, slope, and shelf edifice shaped by sea level and ocean currents, Marion Plateau (Northeast Australia). Am. Assoc. Pet. Geol. Mem. 81, 291–307.
James, N.P., Choquette, P.W., 1990. Limestones – the Meteoric diagenetic environment. In: In: McIlreath, I.A., Morrow, D.W. (Eds.), Diagenesis: Geoscience Canada, vol. 4. Reprint Series, pp. 35–73.
Jo, N., 2013. Open Access Ph.D Thesis. Carbonate Slope Morphology and Sedimentary Processes along Southwestern Great Bahama Bank, vol. 455 University of Miami. https://scholarlyrepository.miami.edu/oa_theses/455.
John, C.M., Karner, G.D., Browning, E., Leckie, R.M., Mateo, Z., Carson, B., Lowery, C., 2011. Timing and magnitude of Miocene eustasy derived from the mixed siliciclastic-carbonate stratigraphic record of the northeastern Australian margin. Earth Planet. Sci. Lett. 304, 455–467.
Karas, C., Nürenberg, D., Tiedeman, R., Garbe-Schönberg, D., 2011. Pliocene Indonesian Throughflow and Leeuwin Current dynamics: implications for Indian Ocean polar heat flux. Paleoceanography 26, PA2217.
Kastens, K.A., 1992. Did glacio-eustatic sea level drop trigger the Messinian salinity crisis? New evidence from ocean drilling program site 654 in the Tyrrhenian Sea. Paleoceanography 7 (3), 333–359.
Keep, M., Bishop, A., Longley, I., 2000. Neogene wrench reactivation of the Barcoo sub basin, North West Australia: implications for Neogene tectonics of the northern Australian margin. Petrol. Geosci. 6, 211–220.
Keep, M., Powell, C.McA., Baillie, P.W., 1998. Neogene deformation of the North West Shelf, Australia. In: Purcell, P.G., Purcell, R.R. (Eds.), The sedimentary Basins of Western Australia 2. Proceedings of the Petroleum Exploration Society of Australia, Perth, pp. 81–91.
Kenter, J.A.M., 1990. Carbonate platform flanks: slope angle and sediment fabric. Sedimentology 37, 777–794.
Kim, W., Fouke, B.W., Petter, A.L., Quinn, T.M., Kerans, C., Taylor, F., 2012. Sea-level rise, depth-dependent carbonate sedimentation and the paradox of drowned platforms. Sedimentology 59, 1677–1694.
Langhi, L., Borel, G.D., 2007. Reverse structures in accommodation zone and early compartmentalization of extension system, Laminaria High (NW shelf, Australia). Mar. Petrol. Geol. 25, 791–803.
Miller, K.G., Janecek, T.R., Katz, M.E., Keill, D.J., 1987. Abyssal circulation and benthic foraminiferal changes near the Paleocen'Eocene boundary. Paleoceanography 2 (6), 741–761.
Miller, K.G., Kominz, M.A., Browning, J.V., Wright, J.D., Mountain, G.S., Katz, M.E., Sugarman, P.J., Cramer, B.S., Christie-Blick, N., Pekar, S.F., 2005. Phaerozoic record of global sea-level change. Science 310, 1293–1298.
Moore, C.H., 2001. Carbonate reservoirs: porosity evolution and diagenesis in a sequence stratigraphic framework. Elsevier Science 55, 1–444.
Mutti, M., Hallock, P., 2003. Carbonate systems along nutrient and temperature gradients: some sedimentological and geochemical constraints. Int. J. Earth Sci. 92, 465–475.
Mylroie, J.E., Carew, J.L., 1990. Flank margin model for dissolution cave development in carbonate platforms. Earth Surf. Process. Landforms 15, 413–424. https://doi.org/10.1002/esp.3290150505.
Mylroie, J.E., Carew, J.L., 1995. Karst development on carbonate islands. In: In: Budd, D.A., Saller, A.H., Harris, P.M. (Eds.), Unconformities and Porosity in Carbonate Strata: AAPG Memoir, vol. 63. pp. 55–76.
O'Brien, G.W., Glenn, K., Lawrence, G., Williams, A., Webster, M., Burns, S., Cowley, R., 2002. Influence of hydrocarbon migration and seepage on benthic communities in the Timor Sea, Australia. APPEA J. Aust. Pet. Prod. Explor. Assoc. 42, 225–240. https://doi.org/10 .1071/AJ01013.
Rosleff-Soerensen, B., Reuning, L., Back, S., Kukla, P., 2012. Seismic geomorphology and growth architecture of a Miocene barrier reef, Browse Basin, NW-Australia. Mar. Petrol. Geol. 29, 233–254.
Rosleff-Soerensen, B., Reuning, L., Back, S., Kukla, P., 2016. The response of a basin scale Miocene barrier reef system to long-term, strong subsidence on a passive continental margin, Barcoo sub-basin. Aust. North West Shelf. Basin Research 28, 103–123.
Saqab, M.M., Bourget, J., 2015. Controls on the distribution and growth of isolated carbonate build-ups in the Timor Sea (NW Australia) during the quaternary. Mar. Petrol. Geol. 62, 123–143.
Schlager, W., 1981. The paradox of drowned reefs and carbonate platforms. Geol. Soc. Am. Bull. 1 (92), 197–211.
Shackleton, N.,.J., Kennett, J.P., 1975. Paleotemperature history of the Cenozoic and the initiation of Antarctic glaciation: oxygen and carbon isotope analyses in DSDP Sites 277, 279, and 281. In: In: White, S.M. (Ed.), 1975. Initial Report Form Deep Sea Drilling Project, vol. 29. pp. 743–755.
Stephenson, A.E., Cadman, S.J., 1994. Browse Basin, North West Australia: the evolution, paleogeography and petroleum potential of a passive continental margin. Palaeogeography, Palaeoclimatology, Palaeoecology 111, 337–366.
Tesch, P., Reece, R.S., Pope, M.C., Markello, J.R., 2018. Quantification of architectural variability and controls in an upper Oligocene to lower Miocene carbonate ramp, Browse Basin, Australia. Mar. Petrol. Geol. 91, 432–454.
Vail, P.R., Hardenbol, J., 1979. sea-level change during the tertiary. Oceanus 22, 71–79.
Van Sickel, W.A., Kominz, M.A., Miller, K.G., Browning, J.V., 2004. Late Cretaceous and Cenozoic ssea-level estimates: backstripping analysis of borehole data, onshore New Jersey. Basin Res. 16 (4), 451–465.
Van Tuyl, J., Alves, T.M., Cherns, L., 2018. Geometric and depositional responses of carbonate build-ups to Miocene sea level and regional tectonics offshore northwest Australia. Mar. Petrol. Geol. 94, 144–165.
Vannucchi, P., Ranero, C.R., Galeotti, S., Straub, S.M., Scholl, D.W., McDougall-Ried, K., 2003. Fast rates of subduction erosion along the Costa Rica Pacific margin: implications for nonsteady rates of crustal recycling at subduction zones. J. Geophys. Res. 108 No. B.11.
Veevers, J.J., Powell, C.McA., 1984. Dextral shear within the eastern Indo-Australian plate. In: Veevers, J.J. (Ed.), Phanerozoic Earth History of Australia. Claredon Press, Oxford, pp. 102–103.
Warrlich, G.M.D., Waltham, D.A., Bosence, D.W.J., 2002. Quantifying the sequence stratigraphy and drowning mechanisms of atolls using a new 3-D forward stratigraphic modeling program (CARBONATE 3D). Basin Res. 14, 379–400.
Warrlich, G., Bosence, D., Waltham, D., Wood, C., Boylan, A., Badenas, B., 2008. 3D stratigraphic forward modeling for analysis and prediction of carbonate platform stratigraphies in exploration and production. Mar. Petrol. Geol. 25, 35–58.
Willis, I., 1988. Results of exploration, Browse basin, North West Shelf, western Australia. In: Purcell, P.G., Purcell, R.R. (Eds.), The Northwest Shelf, Australia: Proceedings of Petroleum Exploration Society Australia Symposium Perth, pp. 259272.
Woodroffe, C.D., Webster, J.M., 2014. Coral reefs and sea-level change. Mar. Geol. 352, 248–267.
Zachos, J.C., Pagani, M., Sloan, L., Thomas, E., Billups, K., 2001. Trends, rhythms, and aberrations in global climate 65 Ma to present. Science 292, 686–693.